Supersonix Inc.

Conceptual Design Review

Of a high speed commercial air transport

Akshay Ashok, Nithin Kolencherry, Steve Skare, Michael McPeake, Muhammad Azmi, Richard Wang, Mintae Kim, Dodiet Wiraatmaja, Nixon Lange

4/30/2009

Table of Contents

Table of Figures

List of Tables

Executive Summary

A high speed supersonic transport was developed in response to NASA's 2008-2009 student challenge. A complete conceptual design has been performed for the aircraft with an Initial Operating Capability in 2020. The aircraft is configured for cruise at Mach 1.8 with a 4500 nautical mile range and a payload of 59 passengers plus 4 crew members. The aircraft has a wing area of 3092 square feet, a takeoff gross weight of 308,000 lb, and four state of the art conceptual low bypass-ratio turbofan engines capable of producing a combined 154,000 pounds of thrust. The engines yield a sea level thrust to weight ratio of 0.5 and wing loading of 100 psf. This report presents the details of a complete conceptual design including sizing, aerodynamics, structures, mission performance, and cost analysis.

The feasibility of this endeavor has been considered from consumer viewpoint in a Systems Requirements Review, and the aircraft took on a more technical definition in the Systems Definition review. Finally, the Conceptual Design Review is performed: A detailed sizing code is developed that allows the optimization of the aircraft; various aspects of the properly sized aircraft such as weights and balance, structures and costs are analyzed to solidify the aircraft concept further. The following table presents, at a glance, the major design parameters of the Supersonix aircraft.

Design Parameter	Value	Units
Aircraft MTOW	308000	lbs
Fuel weight fraction	0.567	
Empty weight fraction	0.433	
Wing area	3092.37	square ft
Wing loading	99.6	lb per square ft
T/W (sea level)	0.5	
Aspect Ratio	2.2	
Aircraft length	200	ft
Strake sweep	70^o	
Outboard wing sweep	36^o	
Thickness to chord ratio	10%	
root chord	85	ft
Taper ratio	0.12	

Introduction

Over the last few years, air traffic has seen a high increase in capacity, range and efficiency. In addition to these, the need for a faster aircraft is imperative at the present time. Transporting people over a longer distance within a shorter span of time will be the objective of the airline industry in the near future. This report addresses the conceptual design of a supersonic aircraft that would have initial operating capability (IOC) in 2020. Conceptual design of an aircraft involves many different steps. The results of those steps are presented in this report. The Supersonix aircraft was sized using a program created in MATLAB. This program was made up of components that evaluated each performance parameter of the aircraft while solving for the smallest maximum takeoff weight.

Creation of an environmentally friendly aircraft is an important design parameter. The high Mach number which the Supersonix aircraft will travel at will create the sonic boom overpressure at sea level. Reducing noise and disturbance, this boom signature must be limited. Work was done to analyze and choose the most efficient aerodynamic shape. The sonic boom of the aircraft was approximated using methods described by Carlson and Seebass. Sonic boom approximation by Seebass provided a rough estimate of boom overpressure using simply aircraft weight; more in depth analysis was done using Carlson which considers geometric parameters and area distribution of the aircraft. Iteration of design yields an aircraft that satisfies the design mission of 4500nm cruise, 2.89 passenger miles per lbs, and an overpressure of 0.28.

Control surface area was estimated by using analysis done by Dr. Roskam[21], and equations in his book were utilized to analyze Longitudinal and lateral dynamic stability. The necessary surface area of the canard, vertical tail, and rudder was determined using simple numerical approximations at first, and then a more through method was used after the sizing code was run. Key constraints necessary for the aircraft to operate safely under normal flight conditions were analyzed for each aircraft configuration. From the thorough analysis of each aircraft sub component came a concept that both satisfied major requirements set in the opportunity description.

Opportunity Description

NASA ARMD 2008-09 University Competition provides a framework that is used to guide the conceptual design of a supersonic aircraft. The aircraft is expected to meet a set of goals specified by the competition. These include, but are not limited to:

- Mach cruise speed of 1.6 -1.8
- Design Range of 4000 nautical miles

- Accommodate 35-70 passengers (preferably in a mixed class configuration)
- Fuel efficiency of 3 passenger-miles per pound of fuel or better
- Takeoff field length < 10,000 ft

Additionally, the aircraft is expected to achieve supersonic cruise efficiency, have a low sonic boom (<70 PldB) and high lift for takeoff or landing – all while making a reasonable profit for the company.

Mission Statement

The Supersonix mission statement is as follows:

A cost-effective, advanced, high-speed commercial air transport that connects major worldwide hubs

Supersonix has set out several key design goals that is expected to be met and exceeded through the course of the conceptual development:

- Supersonic flights over land (boom overpressure less than 0.3 lb/ ft^2)
- Capture significant market of Supersonic Business Jets and supersonic transports
- Initial Operational Capability (IOC)in 2020
- Manufacturing capabilities exist for the aircraft
- Payload of 60 passengers in a twin class configuration
- Still-air ground range of 4500nm

Market Analysis and Concept of Operations

Three focus markets emerge from the market analyses: Trans-Continental, Trans-Atlantic and Inter-Asia. Through detailed studies on market viability and cost models, potential worldwide hubs are selected to set forth a viable business proposition for customer airlines. These are: Los Angeles International Airport (LAX), John F. Kennedy International Airport (JFK), London Heathrow International Airport (LHR), Dubai International Airport (DXB) and Beijing International Airport (PEK). A hub and spoke structure is to be employed, with the reliance on the growing number of Low Cost Carriers to provide regional connections.

Selected Aircraft Concept

The Supersonix concept aircraft boasts many important features designed to address the mission objectives set early in the project. Table 1 gives a brief overview of key design parameters. The aircraft's maximum takeoff weight of 308,000 lb includes 60 passengers and 3 crew members with luggage. The aspect ratio and wing area are appropriate for subsonic and supersonic flight. Generally, these figures are based on historical data for supersonic aircraft,

with important modifications and tweaking in order to meet the specific requirements for the aircraft.

Design Parameter	Value	Units
Aircraft MTOW	308000	lbs
Fuel weight fraction	0.567	
Empty weight fraction	0.433	
Wing area	3092.37	ft^2
Wing loading	99.6	psf
T_{sl}/W_0	0.5	
Aspect Ratio	2.2	
Strake Sweep	70^o	
Aircraft length	200	ft
Outboard wing sweep	36^o	
thickness to chord (mean chord)	10%	
root chord	85	ft
Taper ratio	0.12	

Table 1: Key Design Parameters

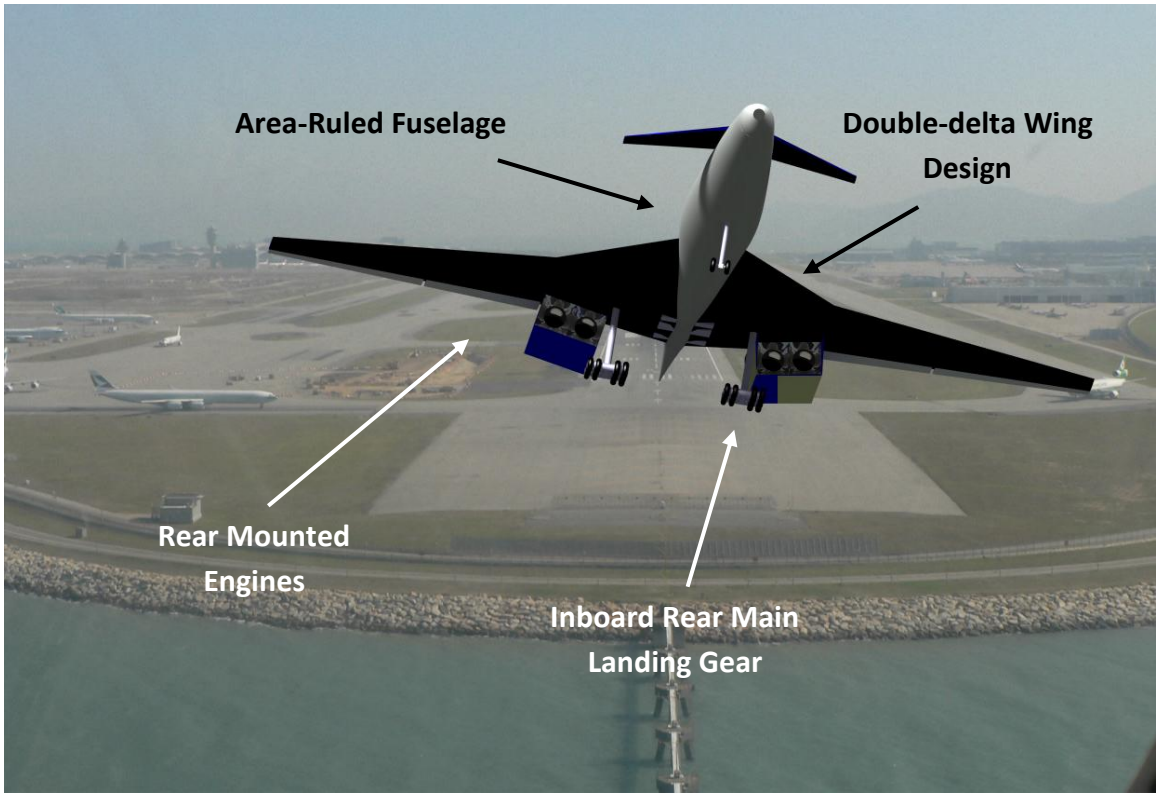

Figure 1: Lower Walk-Around (Takeoff Climb Phase)

Figure 1 above gives a brief walk-around of the aircraft underside. The fuselage shaping is governed by area ruling in order to minimize wave drag. The double-delta wing design features two sweep angles designed to give good flying characteristics for both subsonic and supersonic flight. Engines are mounted on the rear, extending back behind the wing for passenger safety. The engines are mounted below the wing allowing for easy maintenance access, leaving room for the rear main landing gear inboard between the engines and empennage.

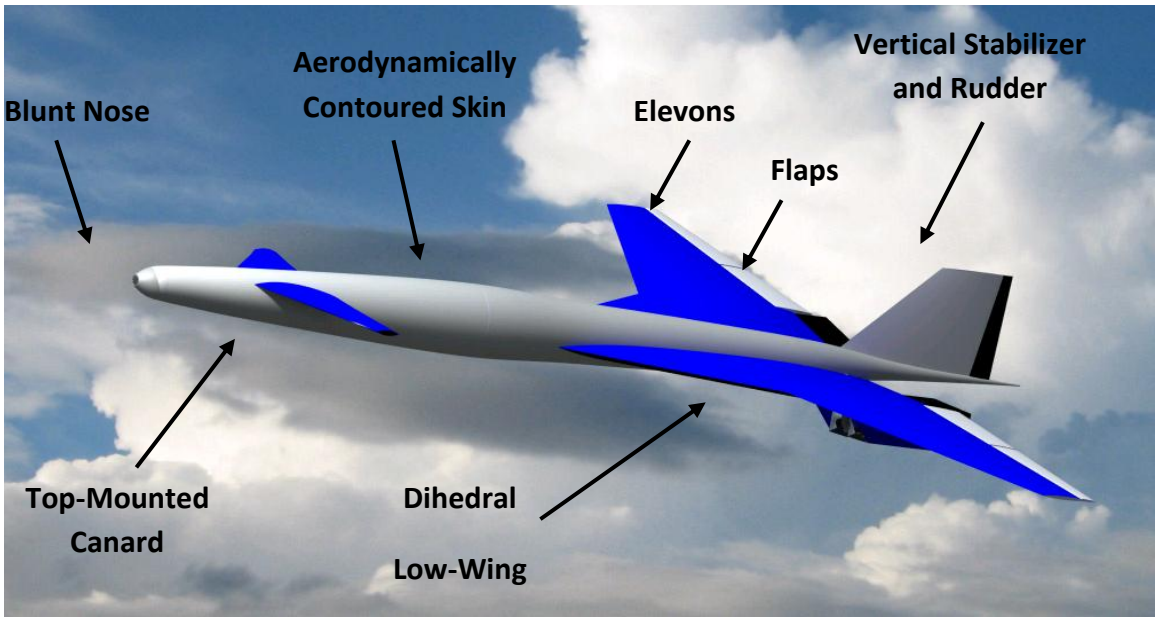

Figure 2: Upper Walk-Around (Approach/Descent Phase)

Figure 2 gives a brief walk-around of the main aircraft features. Aerodynamically contoured skin is designed to minimize wave drag and the blunt nose is designed to significantly reduce sonic boom overpressure as a tradeoff with drag. The top-mounted canard provides additional longitudinal stability, with elevons available for pitch and roll control, and a rudder for yaw control. Inboard flaps can be retracted for the takeoff, approach, and landing phases of flight in order to provide additional lift for these slower flight regimes.

Aircraft Design Mission

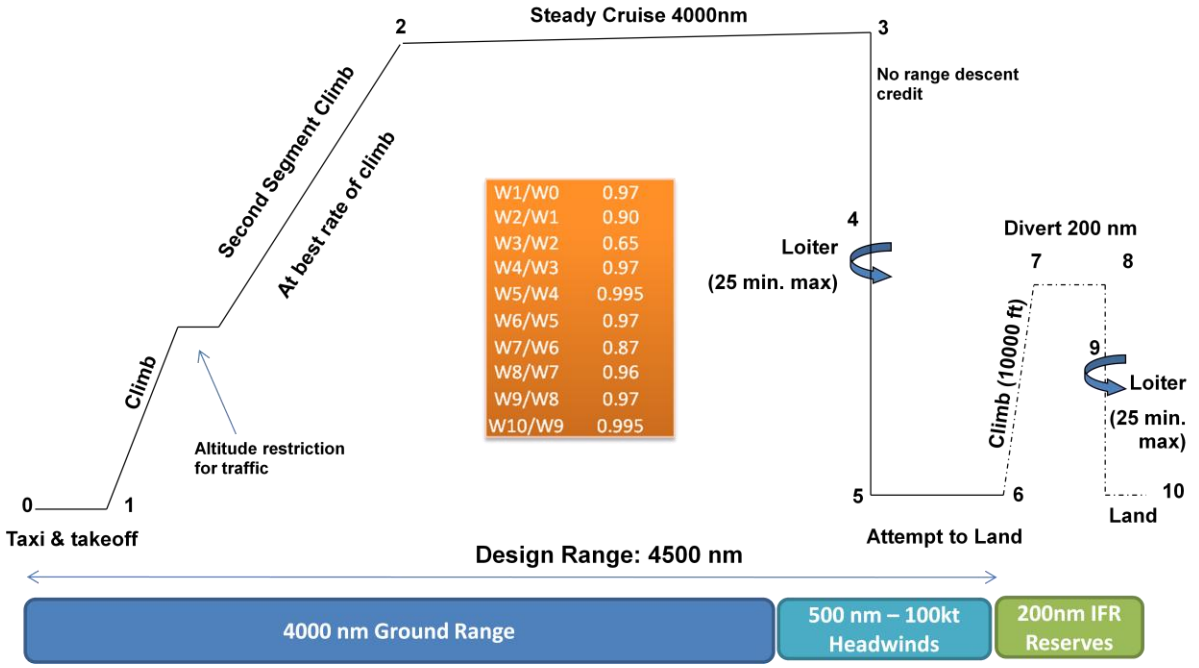

Figure 3: Aircraft Design Mission

Figure 3 above represents the typical mission profile for the aircraft. Supersonix will climb to cruise altitude at best rate of climb right after takeoff. The mission profile has accounted for air traffic control altitude restrictions in order to clear any traffic in the airspace if necessary. This is important especially when flying out from busy airports that are major worldwide hubs. The aircraft will then continue in a steady level cruise for 4000 nm at an altitude of 60000ft. The especially high altitude is essential to the achievement of a low sonic boom overpressure, as will be discussed in the sonic boom section. The mission profile takes into account a 100kt sustained headwind. Though seemingly excessive, this will provide the aircraft with a comfortable margin under the worst-case scenario. If the first attempt to land fails, the aircraft will climb back to 10000 ft and cruise at Mach 0.5 to the next airport that could be up to 200 nm from the first airport. The mission profile includes a total loiter duration of 50 minutes in order to comply with FAA regulations. The endurance time for loiter is split between two loiter periods, one during the normal descent and landing phase and another during the alternate diversion. This is done so that the aircraft can either loiter for 50 minutes and come to a full-stop landing, or divert after 25 minutes to the alternate airport where it has the capability to loiter for another 25 minutes before landing.

Aircraft Detailed Sizing

The sizing code was designed to minimize the maximum takeoff weight of the Supersonix aircraft. To find the most efficient design, thrust to weight, wing loading, and aspect ratio were all iterated through to give detailed information on what the aircraft is capable of doing in different configurations. For each aircraft configuration the program iterated three functions: A/C Geometry, Mission Segments, and Component Weights to find the maximum takeoff weight of the aircraft. Then five functions that computed performance qualities were evaluated. These qualities include the sonic boom overpressure, the airfoil lifting characteristics, core design constraints, stability of the design, and wing loading. The following figure illustrates the design of the sizing program.

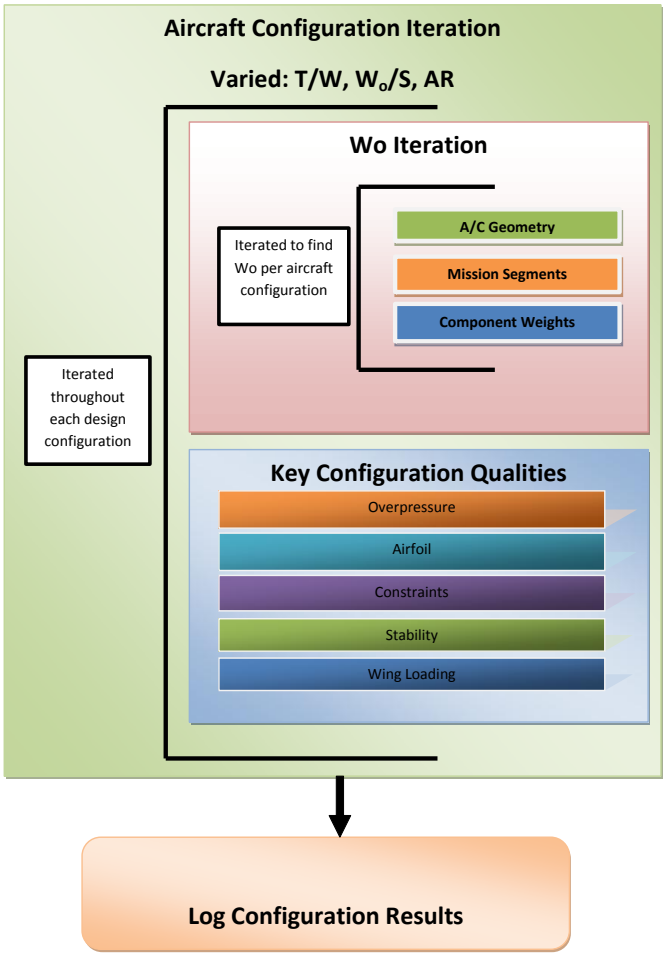

Figure 4: Sizing Program Flowchart

The geometry of the aircraft changed for each configuration iteration. This is because the iteration varies wing loading and aspect ratio. Both of these qualties have significant effects on the overall design of the wing. A more in-depth description of how the functions in the program are designed follows in the Primary Functions section.

Primary Functions

The primary functions are the functions in the Supersonix sizing code that use mathematical methods and assumptions to deal with each of the major design qualities of the aircraft. These include the geometry of the aircraft, the sonic boom that the aircraft produces, and the mission segments that the aircraft must fly on.

A/C Geometry

The objective of the aircraft geometry function was to produce a mathematical representation of the aircraft that could dynamically change given a few key aircraft characteristics. The function used aspect ratio and wing loading to calculate the second wing sweep and total wing area. The radial distribution of the fuselage was hardcoded such that the fuselage had the same shape for every aircraft configuration. If the radial distribution of the fuselage resulted in extreme results, then the values would be changed; however they were not changed in an iterative manner primarily because of the increase in computation time associated with adding the extra complexity. With the wing and fuselage modeled, the function then took a normal cross sectional area distribution and exported that to other programs. This program then returned the area distribution and a wireframe representation of the aircraft to the user. It is important to note that the mathematical representation of the aircraft was three dimensional; thus wings had a thickness defined by the t/c ratio and the fuselage had a cross sectional area distribution determined by the radial distribution over the aircraft length.

To make this function work properly, it was necessary to hold several values constant. The strake sweep was 70 degrees, mean t/c was 10%, length of a/c was 200ft, and the starting locations of the wing, engine nacelle, vertical tail and canard were all held constant. The overall aircraft geometry should have been varied in a more comprehensive manner to yield a more dynamic and detailed model; however given the time constraints for computation and project deadlines, it was infeasible to implement such a sizing algorithm. Without this function, the area distribution would need to be assumed unchanged. This is incorrect, and therefore this function caters to the program by providing a more accurate area distribution of the aircraft which changes with each aircraft configuration iteration.

Mission Segments

As per the mission segments presented earlier in the Design Mission section, the mission function is split into 10 parts. These parts are: taxi and takeoff, climb 1, cruise, holding pattern 1, landing, missed approach, climb 2, divert to alternate, holding pattern 2, and landing. Each flight condition has assumptions that go with it; these assumptions will be presented below. It is important to note that for each flight condition, drag and thrust was calculated, whereby the aircraft is either accelerating or in an equilibrium.

Taxi and Takeoff

A fuel weight fraction of 0.97 was assumed for this segment of the mission. It is based on historical values presented in Raymer[1] (Table 3.2 pp 21).

Climb 1

This is full throttle flight and the aircraft accelerates to cruise speed in a linear fashion.

Cruise:

This segment is flown at partial throttle and the aircraft flies at constant altitude. This is a change from our earlier mission segment of a cruise climb (as in our SDR), and was done because our cruise altitude increased to 60,000ft. A cruise climb would be impractical at this altitude as it is quite high to begin with, and therefore this change was effected.

Holding Pattern 1

The ratio of L/D is assumed to be constant over this flight condition. The aircraft will be flying using partial throttle at Mach 0.4.

Landing

Approximating the landing fuel consumption was done using Raymer[1] (Table 3.2 pp 21).

Missed Approach

Approximating the missed approach fuel consumption was done the takeoff data provided by Raymer[1] (Table 3.2 pp 21).

Climb 2

The second climb was modeled at full throttle up to Mach 0.4 and 10000ft. The climb rate was assumed to be 1200 fpm.

Divert to Alternate

This segment of the mission was flown at partial throttle at 10000ft and Mach 0.4.

Holding Pattern 2

The second holding pattern was flown at Mach 0.4 and altitude 10000ft. The length of this segment was much shorter than the Divert to Alternate segment.

Landing

Approximating the landing fuel consumption was done using Raymer[1] (Table 3.2 pp 21).

Component Weights

To accurately model the component weights of the aircraft, weight equations were used to approximate the different components of the aircraft. The equations used were obtained from Raymer[1] (Chap.15). The book outlines component weights for both military and air-transport vehicles. A combination of these equations was used in the sizing for each component. A more

thorough description of how each type of equation was used is presented later in the report under the Weights and Balance Section.

Overpressure

The sizing code used two numerical approximations for determining the sonic boom overpressure created by the aircraft. Two papers written by Carlson[2] and Seebass[3] outlined numerical methods for approximating the sonic boom overpressure created by the aircraft. These numerical models were integrated into the sizing code and iterated for each aircraft configuration. The two numerical models were used in parallel because they each predicted a different type of sonic boom signature. The Seebass method predicted the plateau wave sonic boom signature, while the Carlson method predicted the N-wave sonic boom signature.

Each method required different data to predict the sonic boom overpressure. Carlson required a cross sectional area distribution, while Seebass required basic aircraft dimensions including takeoff gross weight. From Seebass[3] it was seen that for a supersonic aircraft, it would be more desirable to have a plateau wave rather than an N-wave pressure distribution as it spreads the overpressure over a finite period of time. This would result in a lower average sonic boom overpressure and thus a smaller sonic boom signature. The objective of this function was to give the user an idea on what kind of sonic boom overpressures the aircraft configuration would produce for these two boom signatures. This function completes that objective by using two different numerical models to predict the resulting pressure wave. A more detailed analysis of the methods used and the results from the sizing process is presented in the Sonic Boom section.

Airfoil and Lift Coefficients

The Airfoil function takes in the geometry of the new wing and calculates the $C_{L,max}$ at takeoff and landing. This is necessary for calculating the landing and takeoff field lengths in the Constraints function. A more detailed description on how this function works is outlined in Aerodynamics section.

Constraints

The constraint function evaluates the configuration for seven different constraints. These constraints include: 1G steady level flight, landing and takeoff ground roll for Dubai and JFK airports, second segment climb gradient, and a subsonic 2g maneuver. The Constraint function gives the user the specific excess power at cruise, takeoff and landing distance for Dubai and JFK airports, and the climb gradient and specific excess power during the 2-g maneuver. The results of this function can be seen in the carpet plot section.

Stability

The stability function is used to evaluate the longitudinal stability of the aircraft configuration. Given the geometry of the wing and fuselage, the function calculates the position of the center of gravity and the static margin at both supersonic and subsonic flight. A more detailed analysis of how the stability problem was analyzed is presented in Stability and Control section.

Wing Loading

The wing loading function was used to find the forces that act on the wing and landing gear. The aerodynamic forces are calculated by assuming that the lift acts at the quarter chord throughout the span of the wing. Then the length of the landing gear is calculated given angle of attack restrictions. Furthermore, the loads present on the landing gear were calculated for landing and taxi before takeoff. For a more detailed description of how this function works and how its assumptions affected results, please read Structures section.

Auxiliary Functions

Auxiliary functions are functions that were necessary for the implementation of primary functions. This includes the modeling of the engines and drag approximation. What follows are detailed explanations on how each component was modeled.

Engine Modeling

To accurately size an aircraft it is important to be able to model its engines. This is primarily due to the need for different fuel consumption data during the many different parts of the design mission. Several steps were used to model the engines in the Supersonix sizing code.

We first started out with analyzing the performance of a well known engine that has successfully been in service, the Samara NK-321. Because this engine is from Russia, it was difficult to get design information for its sub components. With the limited information, we then tried to model the Samara NK-321's performance in the program ONX-OFFX. This program was able to simulate the performance of each sub-component, but not iterate through enough performance conditions to provide a useful result. Thus, we decided to utilize the engine performance curves in the back of Raymer [1] (Appendix E). The engine described in the back of the book is roughly similar to the NK-321; however it had more information regarding its basic performance parameters. To import the engine performance engine data to the sizing code we scanned the graphs into the computer and used a program called Digitizer to write out 6^{th} order polynomial functions that directly reproduced the engine performance data in the book. The graphs from the back of the book and the resulting equations that were used to approximate the real performance data are presented in the appendix and Figure 5 (below) respectively.

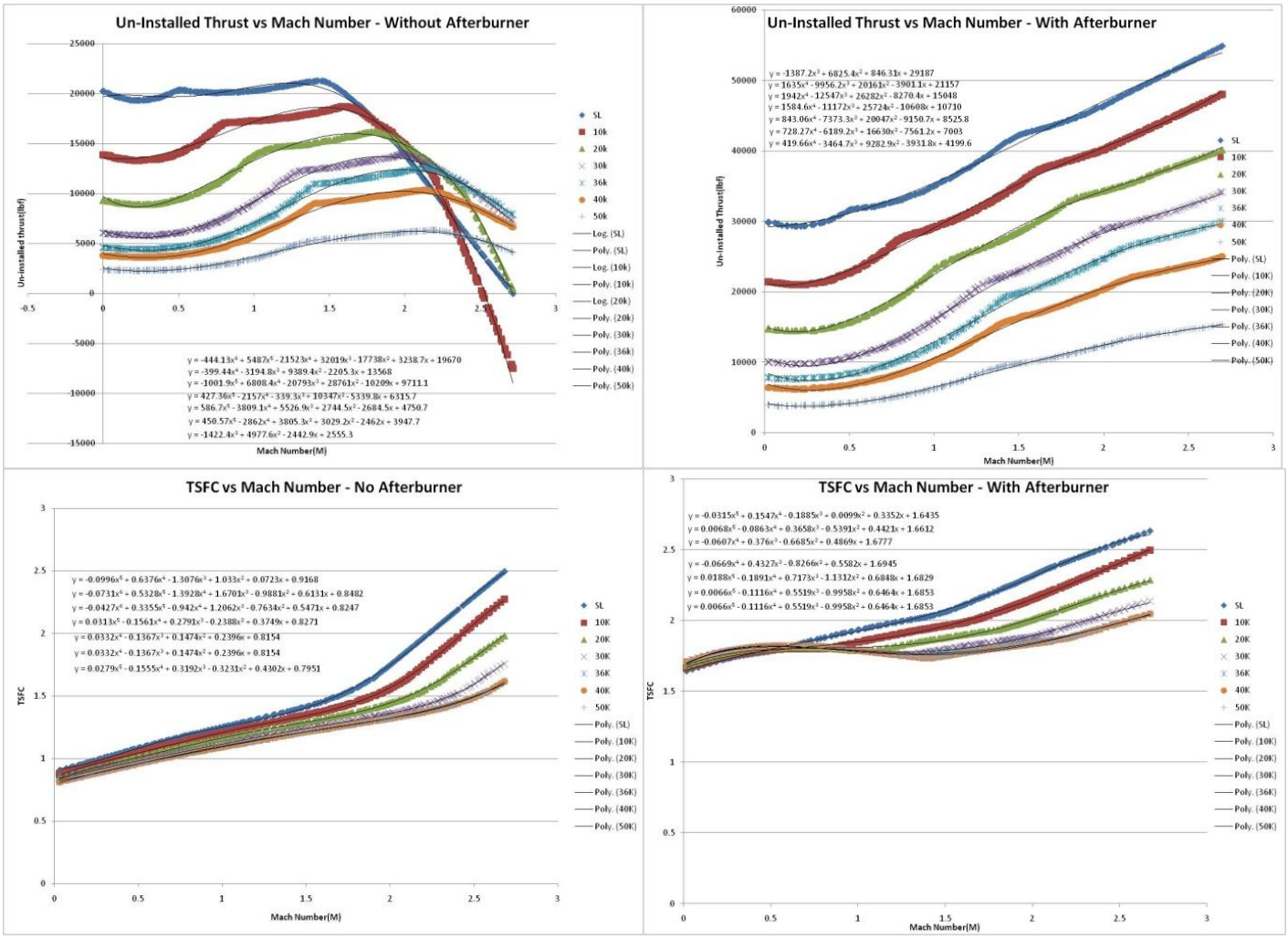

Figure 5: Engine Performance Equations

Note that the engine data depicted above is for when the engine is at full throttle. The colored lines represent the data taken from the back of the book. Where data lines were not present, interpolation was done for the lines above and below the performance point. It was only necessary to model the engine when at full throttle because when the engine was at partial throttle it had constant values of un-installed thrust and TSFC for the Mach range that we would be flying in. Thus, we were able to simply pull the constant values off of the graphs and bypass the process of reverse engineering the performance curves. Two functions were created from these performance curves, one that integrated the performance curves during full throttle and another that used the constant values for use when the engine is at partial throttle.

It is also important to note that the performance curves in the back of the book are for uninstalled thrust. This is significant because the engine inlet and nozzle design can contribute significantly to the overall efficiency of the engine. In order to simulate the addition of a nozzle and engine inlet, it was assumed that when the engine was installed, it would use the same

amount of fuel as if it were only providing 40% of the required thrust for supersonic flight and 80% of the thrust for subsonic flight. These numbers are reasonable considering the Concorde's performance parameters[4], and thus are an acceptable place to begin.

The sizing code scaled the engine model depending on the thrust to weight ratio entered by the iterative process. This allowed the engines to be modified for whatever the design configuration required. While the scaling process is not exactly accurate, it does represent a fairly accurate model that can allow us to predict in greater detail the performance characteristics of the aircraft in different flight regimes.

Drag Modeling

An accurate prediction of drag is essential to the design of the Supersonix aircraft. For steady level flight, a simple force balance reveals that the thrust that the aircraft must have is equal to the drag that acts on it. This in turn drives the engine selection to satisfy the level flight condition during cruise. Further, the amount of fuel required for the mission is dependent on how much thrust is required, and therefore drag calculations have a great influence on the sizing process of the aircraft. Drag prediction is divided into three phases: subsonic, transonic and supersonic flight regimes. These flight regimes correspond to Mach numbers less than 0.8, between 0.8 and 1.2, and above 1.2 respectively. The following discussion presents the drag prediction methods that are used in each of these regimes.

Subsonic Prediction

Subsonic drag prediction involves the computation of parasite drag using the "drag build-up" methodology, as well as calculating induced drag. Parasite drag is generated primarily from surface roughness or skin friction, and is a result of the viscous forces as the aircraft flies through air. The magnitude of the friction depends on whether the boundary layer over the aircraft surface is laminar or turbulent, and to provide a conservative estimate of drag, a turbulent boundary layer is assumed for this analysis. A skin friction coefficient is computed for each component, using the Schlicting formula for turbulent flow represented in Equation 1. The local Reynolds number is computed from the aircraft Reynolds number through a ratio of characteristic lengths, as given in Equation 2.

$$C_f = \frac{0.455}{\left(\log_{10} Re\right)^{2.58}}$$

Equation 1

$$Re_{comp} = Re_{\infty}\frac{l_{comp}}{l} = \frac{\rho V l}{\mu}\frac{l_{comp}}{l}$$

Equation 2

Pressure drag, or form drag, is another component of parasite drag. This is caused by non-ideal pressure distribution over component surfaces. A form factor, *K*, is estimated for each component and used in the drag prediction. Equation 3, Equation 4 and Equation 5 illustrate the form factors that are computed for the wing, fuselage and nacelle components. Note that *D* represents the diameter of the component, while *l* is the length of that component.

sweep correction factor

$$Z = \frac{(2-M^2)\cos(\Lambda_{c/4})}{\sqrt{1-M^2\cos^2(\Lambda_{c/4})}} \qquad K_w = 1 + Z\left(\frac{t}{c}\right) + 100\left(\frac{t}{c}\right)^4$$

Equation 3

$$\lambda_f = \frac{l_f}{D_f} \qquad K_f = 1 + \frac{60}{\lambda_f^3} + \frac{\lambda_f}{400}$$

Equation 4

$$K_N = 1 + \frac{0.35}{(l_N/D_N)}$$

Equation 5

Since the Supersonix wing is a double-delta form, the wing sweep angle ($\Lambda_{c/4}$) in the sweep correction factor (Z) is averaged between the inboard wing sweep and the outboard sweep. The wing thickness-to-chord (t/c) ratio is assumed to be the mean aerodynamic thickness-to-chord ratio for the wing. Furthermore, because the fuselage exterior cowling diameter is not constant, the maximum diameter is used to compute the fineness ratio for use in the fuselage form factor. This would, once more, produce an over-estimation of the drag of the aircraft.

Interference drag is the third, and final, component that is modeled under parasitic drag. This type of drag accounts for the drag created by separation of flow near intersections or joining of parts. It also accounts for nacelle-fuselage and nacelle-wing interference. In the model, an interference factor Q is utilized to incorporate the effects of interference drag. The selection of the values for Q is more subjective, and range from 1.0 for the best case to 1.5 for the worst case. Because the exact manner of the nacelle attachments is not known, a value of 1.3 is assumed for the nacelle interference factor. The wing is mounted low on the front of the

fuselage, but terminates at a rather mid-fuselage location. To account for this interference, a value of 1.2 was used for Q.

The form and interference factors combine with the skin friction coefficient to yield an estimation for the parasite drag, $C_{D,p}$, that is modeled in the sizing code according to Equation 6. The drag was computed for the different parts of the aircraft, namely the wing, fuselage and nacelles. The wetted area of each component is obtained from the A/C Geometry function in the sizing code. This is important to accurately predicting drag of the Supersonix aircraft, as some geometry such as the variable diameter aerodynamic fairing cannot be approximated by a constant-diameter cylinder. The canards and vertical tail were omitted from the drag prediction as these components were sized after the aircraft sizing process was completed and as such were not well defined during the code iterations.

$$C_{D_p} = \sum_{\text{components}} \frac{K_i Q_i C_{f_i} S_{wet_i}}{S_{ref}}$$

Equation 6

Parasite drag due to lift is known as induced drag. It has been experimentally observed that drag varies with C_L^2, as seen in Equation 7:

$$C_{D,i} = \frac{C_L^{\,2}}{\pi A R e}$$

Equation 7

Oswald's efficiency factor, e, varies between 0.75 and 0.85, and is fairly difficult to predict. For this drag prediction, it is assumed to be 0.8 during subsonic conditions.

Finally, a 3% margin is added to the overall drag prediction to account for inefficiencies in fittings, leakages between flaps and control surfaces, antennas and lights. This is termed miscellaneous drag $C_{D,misc}$.

The various components of drag are brought together by the subsonic drag prediction formula:

$$C_D = C_{D,p} + C_{D,i} + C_{D,misc}$$

Equation 8

Supersonic Drag

Drag prediction in the supersonic regime is set apart from the prediction in the subsonic regime due to the predominant 2-dimensional flow as well as the emergence of shock waves.

Parasite drag is computed using the same equations as in the subsonic regime, except that the form factors and interference factors are ignored (set to 1). This approximation is justified as the flow is mostly 2-dimensional, and lateral interferences between components would be minimal in face of the highly axial flow. Furthermore, pressure drag is modeled as wave drag; therefore form factors can be neglected in parasitic drag. A second modification is made to Oswald's efficiency factor in induced drag computations. Following Raymer's example[1] (Chapter 12 pp 348) the factor is modeled as a function of the flight Mach number and aircraft aspect ratio, as given by Equation 9:

$$e = \frac{(4AR\sqrt{M^2-1})-2}{\pi AR^2\left(M^2-1\right)\cos(\Lambda_{LE})}$$

Equation 9

One of the major components of drag that arises due to shock waves is wave drag. While there are NASA codes that predict wave drag (AWAVE being one of the prominent ones), they require a very detailed description of the aircraft geometry to work effectively. Also, wave drag has to be computed each time the drag code is called in the sizing function, and to have revert to NASA codes each time would mean extended computational wall-time. Therefore, in conjunction with the A/C Geometry function, a wave drag prediction code was developed.

A simplified area-rule methodology, developed by Jumper[5] is used in predicting wave drag. An axis-normal cross-sectional area distribution is obtained from the geometry function, and an equivalent body of revolution is generated based on this area distribution. Then, Jumper proceeds to build an area distribution using Mach-angle cross-sections projected onto a normal plane. This process was not implemented in the current drag prediction, due to its complexity. Instead, the original axis-normal distribution is utilized to compute wave drag as follows:

$$D = -\frac{\rho U_\infty^2}{4\pi}\int_0^1\int_0^1 A''(x_1)\,A''(x_2)\,\ln|x_1-x_2|\,dx_1\,dx_2$$

Equation 10

Where A''(x) refers to the second derivative of the area distribution. The original area distribution has several pointed edges and sharp drops, each of which would prove a hindrance for numerical computation of the second derivatives. Therefore, the curve was smoothed

before computing the derivatives. Second-order central differencing is used for the interior points, while first-order one-sided differencing is used for the boundary points.

Transonic Drag

The bridging of the gap between subsonic drag and supersonic drag is important as the aircraft must be designed to be able to pass through the drag rise. A graphical method presented in Raymer[1] (Chapter 12 pp 341) is used to model the transonic drag. It is clearly understood that his method is a very simplified approximation, and while providing some insight into the behavior around Mach 1, does not represent the true nature of this regime. Nevertheless, given the level of detail of conceptual design, it proves to be a useful and relatively easy tool to model transonic drag.

The critical Mach number is approximated to be 0.8, demarcating between subsonic and transonic regimes. Parasite drag is computed for Mach 0.8 and Mach 1.2, after which the gap between the two is bridged using control points in between, as described by Raymer. The end result is shown in Figure 6:

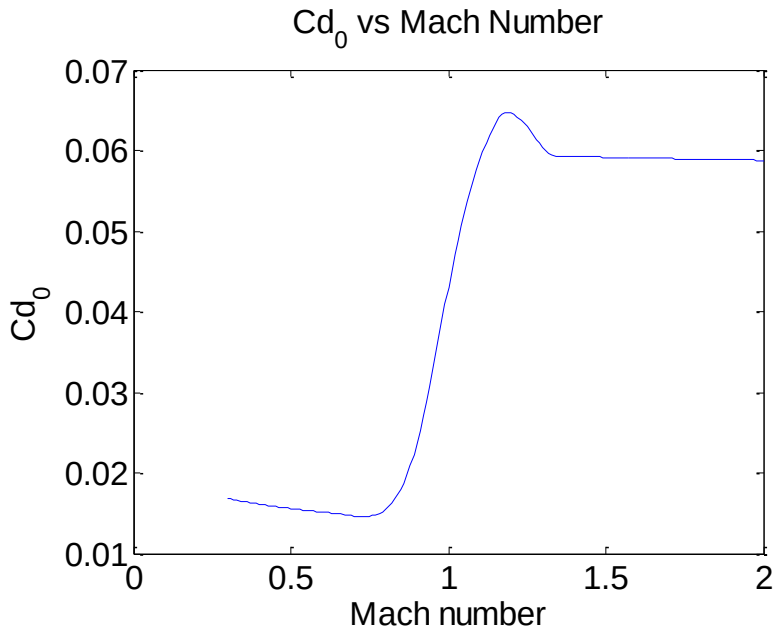

Figure 6: Parasite drag variation with Mach number

The peak drag occurs at about Mach 1.1, the magnitude of which is determined by a smooth curve segment connecting the subsonic parasite drag to the supersonic parasite drag. The ability to predict transonic drag would better enable us to estimate drag, and therefore the amount of fuel required, during the climb segment when the aircraft passes through the sound barrier.

Carpet plot

The sizing code has been run for a variety of aircraft configurations, and a methodical process is required to evaluate the different configurations and choose one or a set of aircraft configurations. As a preliminary tool, a constraint diagram was built and presented in the Systems Definition Review. Whereas the constraint diagram utilizes simplified equations and assumptions to model the aircraft in a more general sense, the carpet plot aims to characterize the Supersonix aircraft in terms of its capabilities and behavior using more detailed models from the sizing code. The objective of the carpet plot is to optimize aircraft takeoff gross weight (W_0) for various aircraft design parameters. The takeoff weight of the aircraft is chosen as the objective variable amongst other metrics, because most of the other metrics are dependent on the aircraft weight. For instance, minimizing aircraft weight would tend to minimize purchase cost or maintenance cost. It is important to note that the carpet plot method is still an approximate process, as it relies on a finite set of data points to characterize the aircraft operation. A better approximation is achieved by discretizing the iterative variables more finely, to an extent that is practical and sufficient for the level of detail required in conceptual design.

Next, the choices for the iterative configuration parameters are considered. In minimizing aircraft weight, there are six key variables that have a great influence on the TOGW of the aircraft: Wing-loading, Thrust-to-weight ratio, Aspect ratio, thickness-to-chord ratio, wing sweep angle and taper ratio. Of these, the first three variables, namely Wing-loading, Thrust-to-weight ratio and Aspect ratio, are chosen to be the iterative variables.

The constraint diagram, which was presented in the Systems Definition Review and is shown in Figure 7, provides a good starting point for the iterative variables. The design point in the constraint diagram is selected to be a wing-loading of 75 psf, and a thrust-weight ratio of 0.5. Using these as ballpark numbers, the range of values for thrust-to-weight ratio, wing-loading, and aspect ratio are chosen to be iterated. This is shown in Table 2. The data is discretized relatively finely to obtain a more accurate solution as described above.

Table 2: Iterative Variable Definitions

Variable	Range of iteration
Thrust-to-weight ratio (T/W)	[0.3,0.6], in increments of 0.1
Wing-loading (psf)	[90,120], in increments of 5
Aspect ratio	[1.9,2.3], in increments of 0.1

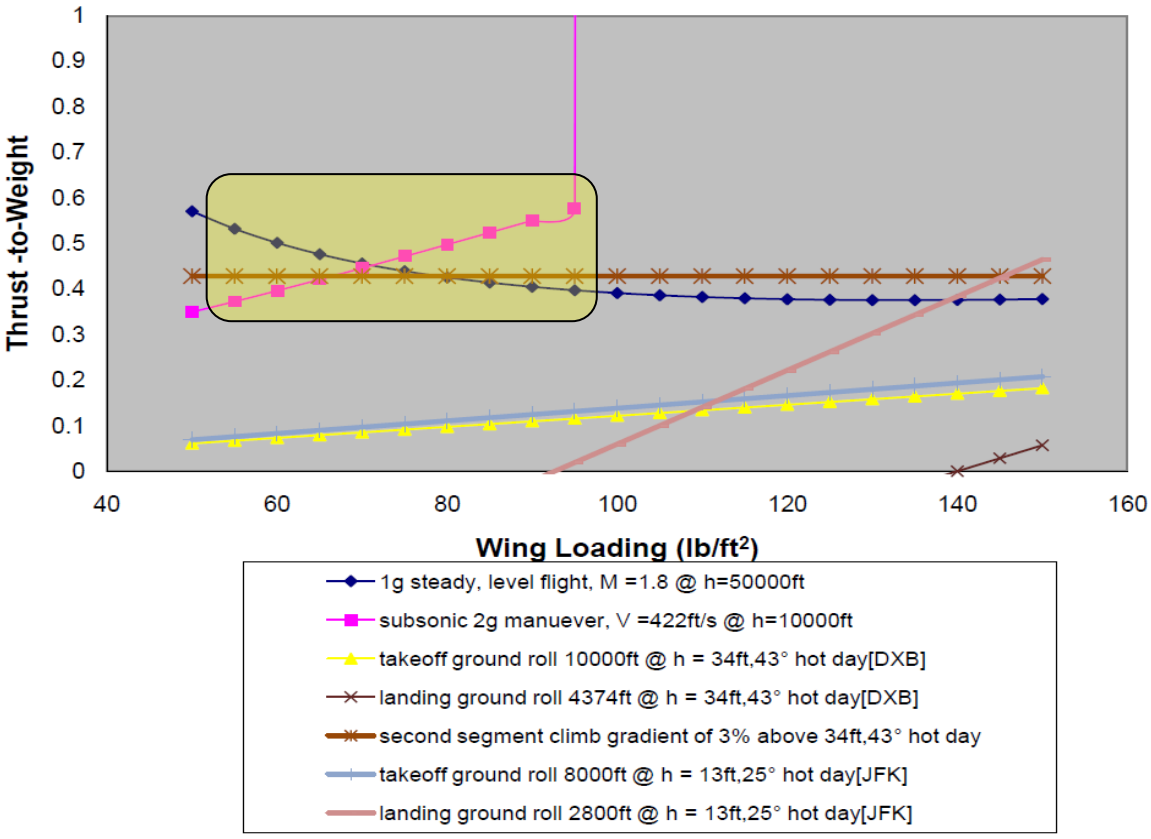

Figure 7: Constraint Diagram from SDR

The carpet plot evaluates the data in terms of constraints that are placed on the aircraft design. Table 3 illustrates the constraints that are imposed on the aircraft design. Some of these constraints, such as the takeoff and landing field lengths, arise due to the design mission of the aircraft. There are two airports that enforce such constraints on performance: J.F. Kennedy (JFK) airport in New York, and Dubai (DXB) airport in Dubai. JFK has the shortest runway amongst the hub airports (8000ft), and to be able to operate from this runway would greatly increase operational capability out of JFK. The hot climate in Dubai also poses a challenge, and it is necessary to be able to operate out of DXB on a hot day.

Constraint	Limits
Takeoff Field length	<8000ft @JFK, <10000ft @ DXB hot day (+15F)
Landing Field length	<2800ft @JFK, <4374ft @DXB hot day (+15F)
Climb gradient	>3.0% for quad-engine configuration
Specific excess power	>0 for subsonic 2-g maneuver, >0 for cruise @60000ft
Specific excess power	<600ft/s for cruise
Overpressure	<0.3 psf during cruise

Table 3: Constraints

The climb gradient constraint is required for compliance with Federal Aviation Authority regulations. The Supersonix aircraft will have 4 engines, and therefore needs to have a climb gradient of at least 3% during its second segment climb segment. The overpressure constraint restricts the boom overpressure to below 0.3 psf. This is essential to the allowance of overland supersonic flight by the FAA, as is expected to occur in the near future.

Yet other constraints, such as the specific excess power during the subsonic 2-g maneuver and cruise, come about as a result of the absolute required performance of the aircraft. The minimum cruise specific excess power of 100 ft/s is necessary for the service ceiling performance. A 2-g maneuver is anticipated to avoid pattern traffic in the process of flying in and out of busy hub airports. A maximum (upper) cruise specific excess power constraint of 600ft/s is also placed on the aircraft. This is done to narrow the design space on the carpet plot and prevent over-designing the engines for unnecessary power during cruise. This will be elaborated on in the discussion of the carpet plot.

These constraints are evaluated for each run of the sizing code, through an automatic filtering process. This filtering process determines the threshold values of the iterative variables for which the aircraft meets the constraints. This data is used to plot constraint curves on the carpet plot.

Figure 8 shows the final carpet plot that is used to pick the design point. Although the sizing code was run for finer intervals of thrust-weight ratios, only a few curves are plotted for clarity. In the interest of time, a “traditional” carpet plot with its offset axes was not created. It is noted that, even though wing-loading is plotted on the abscissa, it is by no means the only independent and important variable in the sizing process. The constraints are calculated and plotted on the same plot to identify the design point. The shaded region depicts a boundary such as a floor or ceiling, and indicates which side of the curve represents the feasible design space. There are fewer constraints that are plotted on this curve than what are highlighted above. These “missing” constraints represent conditions that the aircraft meets and exceeds for all combinations of thrust-to-weight ratios and wing-loading values. As such, only the constraints that actually constrain the design space are plotted. Also, the landing constraint represented here is for the JFK airport. The constraints for takeoff and landing at DXB and for takeoff at JFK are fully met, and therefore do not appear on the plot.

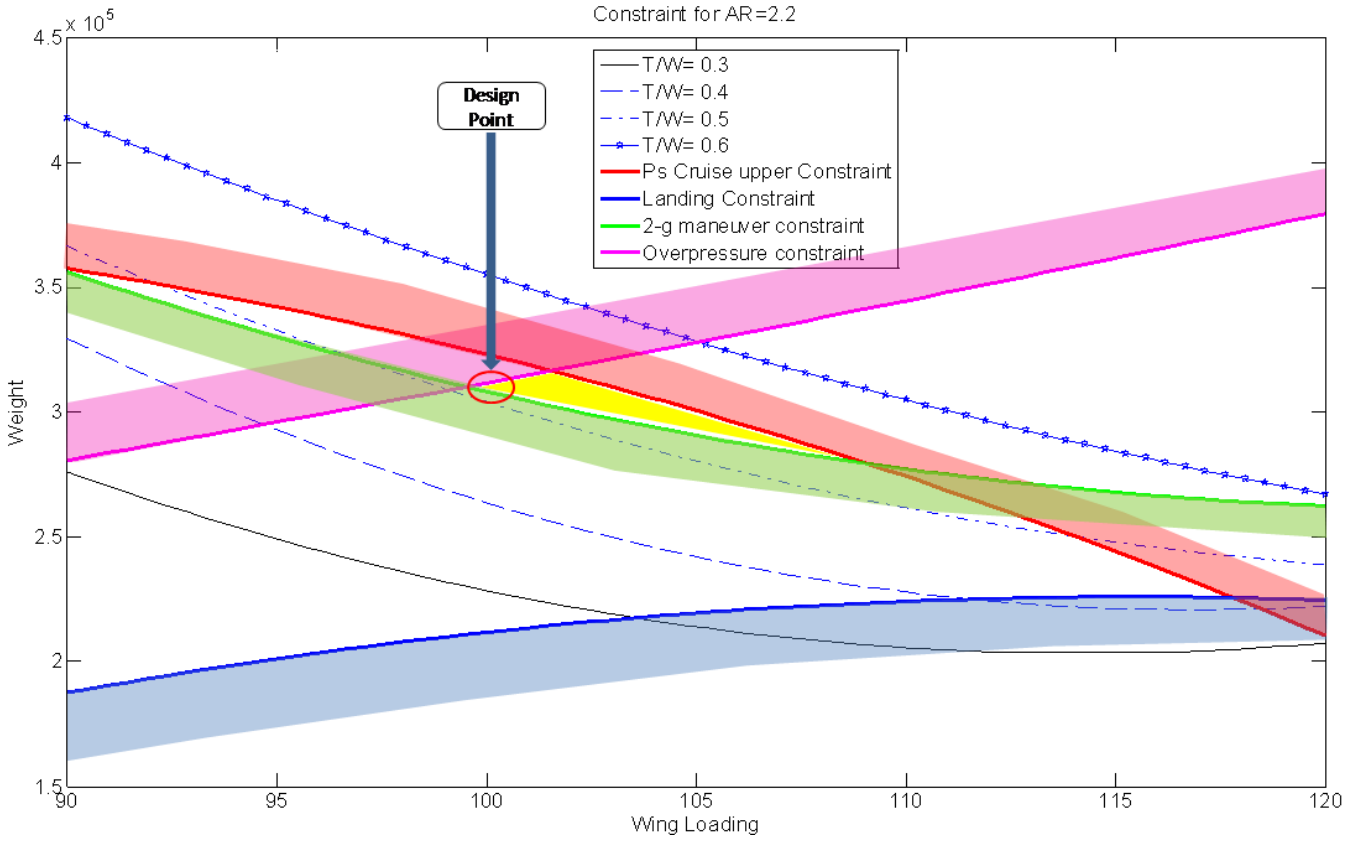

Figure 8: Final Carpet Plot for design point of Supersonix aircraft

The design space is highlighted in yellow, and is bounded by the overpressure, 2-g maneuver specific excess power, and maximum cruise specific excess power constraint. The design point that is chosen for the Supersonix aircraft is marked on the figure, at a wing loading of about 100 psf and the thrust-to-weight ratio of 0.5. At this point, the aircraft weight is clearly not minimized. The red constraint curve representing the upper limit of cruise specific excess power (600ft/s) reveals the reasoning behind this decision. A higher thrust-to-weight ratio yields greater specific excess power during cruise, as evidenced by the shaded side of the red curve. The minimum aircraft weight design point at a wing-loading of about 109 psf results in a thrust-weight ratio of 0.55. The cruise specific excess power at this point is 600ft/s, resulting in an over-powered engine as such extra power is not required during cruise. The design point has a specific excess power of about 500 ft/s, exceeding the service ceiling requirement of 100ft/s while being the lowest that can be achieved considering the rest of the constraints. Therefore, the design point is chosen at the lower thrust-to-weight limit of 0.5, despite yielding a slightly higher aircraft weight.

For a comparison of the effect of aspect ratio on the aircraft weight, a composite carpet plot is created and shown in the appendix. The feasible design space is highlighted in yellow in each subplot. It is clear that, as the aspect ratio gets bigger, the aircraft weight decreases.

Historically, the aspect ratio for supersonic aircraft is around 2.1 according to our database. Therefore, in combination with the composite carpet plot and historical trends, an aspect ratio of 2.2 is selected for the Supersonix aircraft.

Aircraft Concept/Description

Several factors contribute to the cabin layout of the Supersonix aircraft concept. Passengers desire a comfortable and spacious seating environment, but it is important to meet aircraft design constraints and FAA requirements as well. Passengers will be paying a hefty sum of money to fly supersonic on this aircraft, but it is debatable to what extent a passenger will hold seating layout a priority in their travel with such short flight times.

Business analysis has shown that the target customer base values time a bit more than comfort, but at the same time people who can afford to pay for time savings like this generally may expect more from their seating. There is a delicate balance between passenger comfort, safety, efficiency, and aircraft size and shape.

First Class	Coach Class
Seat Pitch: 40”	Seat Pitch: 36”
Seat Width: 28”	Seat Width: 20”
Aisle Width: 28”	Aisle Width:20”
Aisle Height: 6’6”	Aisle Height: 6’6”
No overhead bins	Overhead bins

Table 4: Cabin Layout Dimensions

After analyzing historical data, it is apparent that typical subsonic transports run by the airlines have a maximum seat pitch in first class of about 40 inches, though it is generally much less. Larger specialty aircraft with long flight times may have seat pitches between 55 to even 100 inches or more with fully reclining “sleeper” seats or suites. Generally, supersonic flights will be no longer than 4 hours, so traditional reclining seats appear to be the most reasonable option. For coach, the maximum seat pitch is around 36 inches but the same idea still applies.

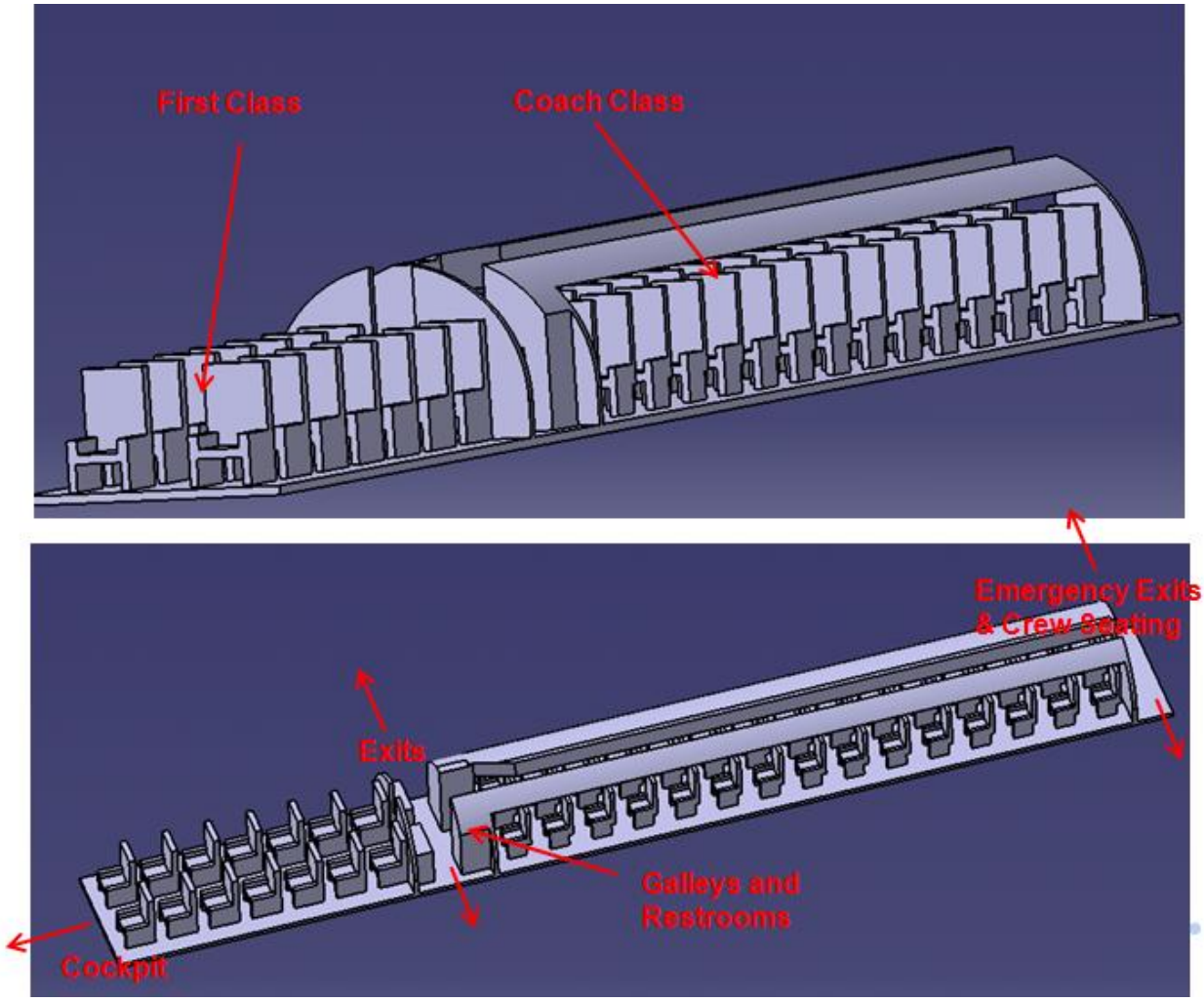

Figure 9: Seating Layout with Galleys and Restrooms

The seating configuration gives first class passengers 7 rows of 2 seats, and gives coach passengers 15 rows of 3 seats for an overall total of 59 passengers. Two flight attendants will have folding "jump seats" available in the rear.

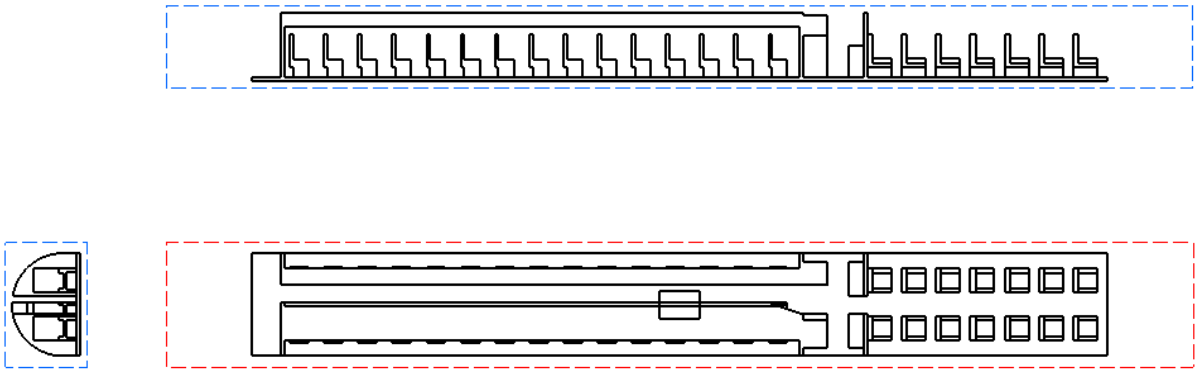

Figure 10: Cabin Three-view Layout

Other parameters, such as aisle and seat width, are also obtained using the method described above. The first class aisle is 28 inches wide, while the coach aisle is 20 inches wide. First class and coach seats are also 28 and 20 inches wide respectively; these values also represent the upper limits for seating in a typical subsonic transport such as a Boeing 737 or Airbus 320. The seat width also takes into account the extra fuselage width available with only 2 seats per row in first class.

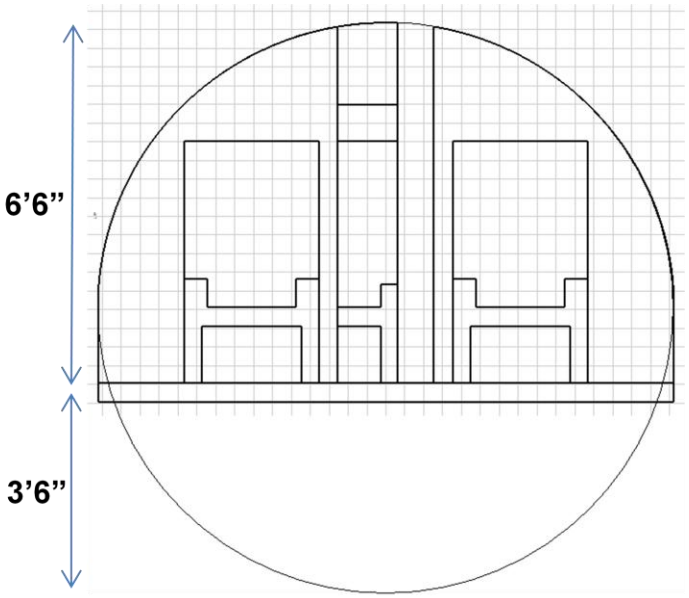

Figure 11: Cabin Cross-section View

Placing the floor 3.5 feet from the bottom of the cylinder allows for a 6.5 foot aisle height. The inner cabin (inner fuselage) is designed as a basic cylinder for easy cabin pressurization. Though this inner section is cylindrical, the idea is that outer fuselage geometry can be built around this cylinder to allow for area rule compliance as well as aerodynamic shaping. Having this inner cylinder should allow more room for adjustability, and it is desirable from a structural standpoint.

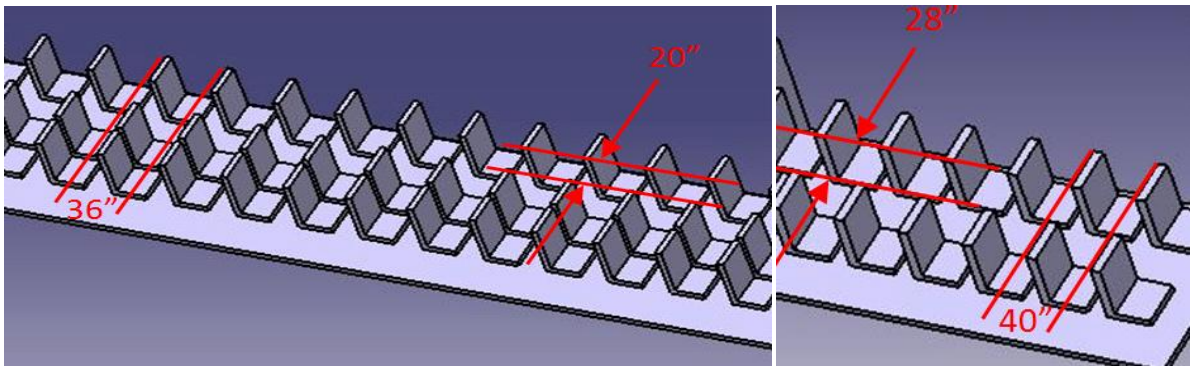

Figure 12: Seating Dimensions, Coach (L) First Class (R)

Aerodynamics

Airfoil Selection

The Airfoil selection process for the Supersonix aircraft requires an in-depth knowledge of airfoil performance in supersonic, subsonic and transonic flight. The wing is the primary source of lift for the aircraft and wing aerodynamics plays a vital role in deciding the aircraft flying qualities. Very little information was available on airfoils suited for the required design mission. For this reason, a database of existing supersonic aircraft along with the airfoils they used was created. Table 5 includes available information[6] on airfoils used in supersonic aircraft. Given the popularity of its application in modern supersonic fighter aircraft, the NACA 6-series and the biconvex airfoils stand out as the best options for the required design mission.

Aircraft	Wing Root airfoil	Wing Tip airfoil
Rockwell D481 B-1 Lancer	NA69-190-2	NA69-190-2 ?
General Dynamics F-111 Aardvark	NACA 64-210.68	NACA 64-209.80
Northrop F-5 Tiger	NACA 65A004.8	NACA 65A004.8
Lockheed Martin F-16 Fighting Falcon	NACA 64A204	NACA 64A204
McDonnell Douglas F-15 Eagle	NACA 64A006.6	NACA 64A203
McDonnell Douglas F-18 Hornet	NACA 65A005 mod	NACA 65A003.5 mod
Grumman G-303 F-14 Tomcat	NACA 64A209.65 mod	NACA 64A208.91 mod
Lockheed 246 F-104	Biconvex 3.36%	Biconvex 3.36%
McDonnell Douglas F-4 Phantom II	NACA 0006.4-64 mod	NACA 0003-64 mod
Convair 4 B-58 Hustler	NACA 0003.46	NACA 0004.08
Convair 8-24 F-106A Delta Dart	NACA 0004-65 mod	NACA 0004-65 mod
Republic F-105 Thunderchief	NACA 65A005.5	NACA 65A003.7
Lockheed/Boeing 645 F-22 Raptor	NACA 64A?05.92	NACA 64A?04.29

Table 5: Airfoils for current supersonic aircraft

Supersonic airfoil analysis is beyond the scope and time constraints posed, and hence could not be done for initial airfoil selection. Since supersonic airfoil analysis could not be performed on the airfoils available, to select the best airfoil for use on the Supersonix aircraft, subsonic constraints were placed. The constraints used for analyzing the best airfoil in subsonic flight are:

1. High C_{Lmax} as required during takeoff and landing.
2. Delayed stall angle.

Subsonic airfoil analysis was done on the NACA 6-series airfoils using the XFOIL subsonic airfoil design and analysis software. This software can only be used to perform analysis for subsonic flight conditions and not for supersonic analysis. Airfoil co-ordinates for various NACA 6-series airfoils were obtained[6]. Geometric information for the biconvex airfoils was not available and for this reason, analysis was only performed on the NACA 6-series airfoils. XFOIL analysis was run on each of the available airfoils and polar files were generated. Lift curve plots (Figure 13) were generated for each airfoil on the same figure for a comparative analysis.

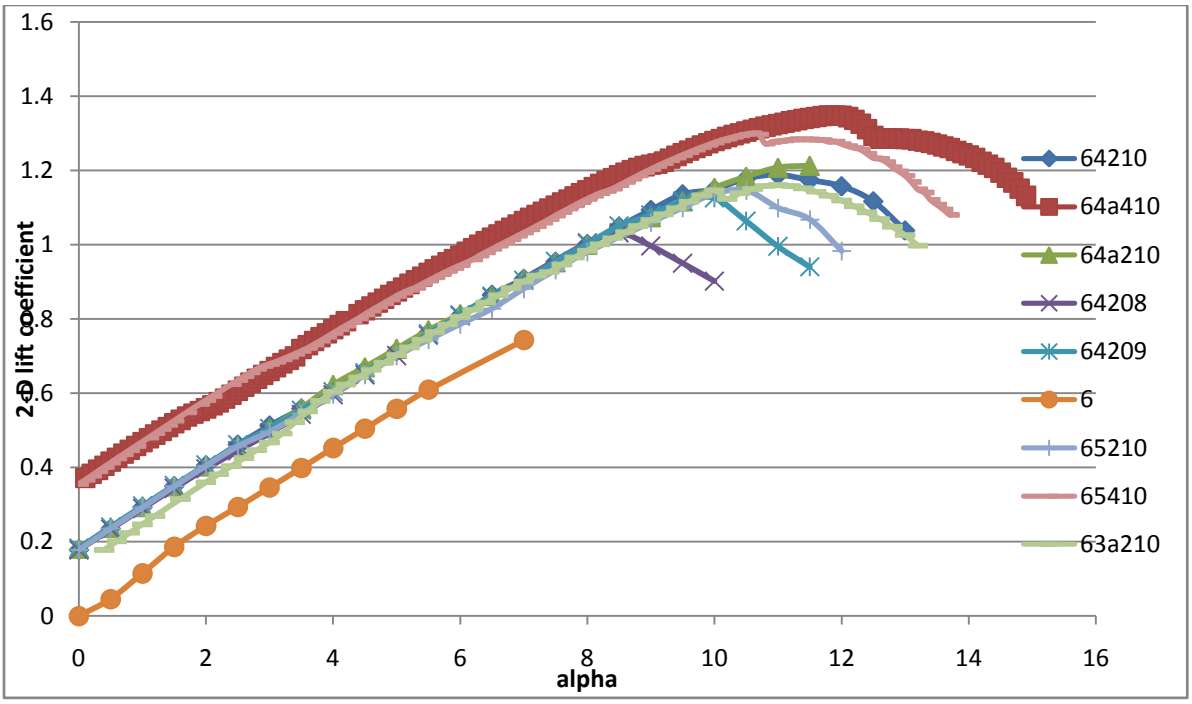

Figure 13: Lift vs angle of attack plots for various airfoils

From the above figure, the NACA 64A410 airfoil was determined to have the best C_{lmax} value at a delayed stall angle of about 12.5˚. This airfoil was selected to be used at the mean aerodynamic chord on the Supersonix wing. From the figure, it is also possible to see how the stall angle decreases with a decrease in the thickness to chord ratio. The profile of the NACA 64A410 airfoil is given in Figure 14. The NACA 64A410 airfoil has a thickness to chord ratio of 10%. This was a major concern because the root chord of the aircraft is approximately 85'. This would give a wing root thickness of 8.5' which is unreasonable given that the fuselage diameter itself is 12'. Therefore, a constant thickness to chord ratio will not be maintained along the span of the wing. There will be a gradual variation in thickness to chord ratio in such a manner that is feasible structurally yet results in adequate performance of the lifting surface. More analysis on the aircraft wing airfoil needs to be done, but it is not necessary at this point in the design phase.

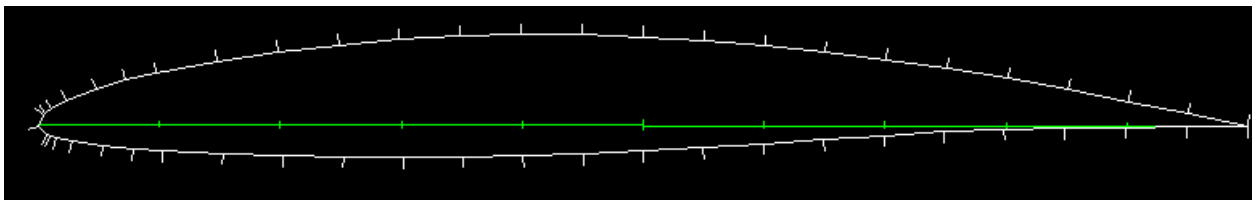

Figure 14: NACA 64A410 airfoil

The lift curve slope for the selected airfoil was 0.1 per degree and it had a zero lift angle of -3.44˚. This had to be corrected for the aspect ratio and taper ratio of the wing, to account for

finite-wing 3-d effects. The aspect ratio for the Supersonix aircraft wing is 2.2 and the taper ratio is 0.12, decreasing the lift curve slope to 0.05 per degree. Calculation of the corrected lift curve slope was done using the formula,

$$a = \frac{a_0}{1 + \left(\frac{a_0}{\pi AR}\right)(1 + \tau)}$$

Equation 11

where a, a_0 are the lift curve slopes in per radian for the wing and the airfoil respectively. A lift efficiency factor τ of 0.04 was assumed. This aspect ratio correction resulted in a wing with a clean C_{Lmax} of 0.8373 and the same zero lift angle of -3.44˚. Figure 15 shows the 2-D airfoil and 3-D wing lift curves.

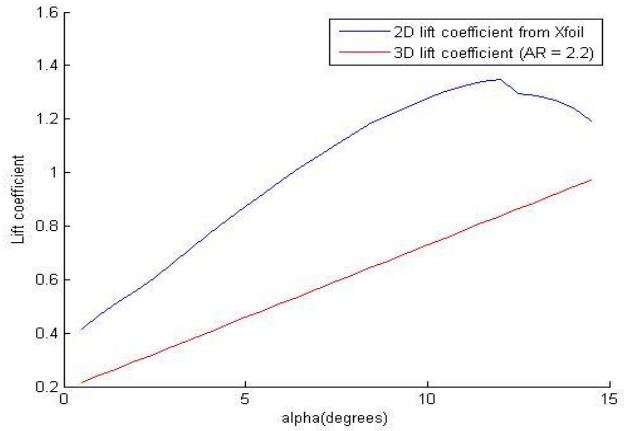

Figure 15: Corrected lift-curve

The C_{Lmax} required by the aircraft is dictated by the takeoff and landing performance. For this reason, the C_{Lmax} that the wing is required to achieve was set to be the C_{Lmax} required by the aircraft during landing and takeoff. This value of C_{Lmax} required was calculated using the equation

$$C_{L\max} = \frac{L}{\frac{1}{2}\rho v^2 S}$$

Equation 12

where L is equal to the weight of the aircraft under that flight condition, S is the wing planform area, ρ is the density and v is the flight velocity for the particular flight scenario. For the landing configuration, the flight velocity was set to be 170 knots. Typically this value would be set by

the selection of high lift devices, and/or airfoils. By setting a specific landing velocity and thereby computing a suitable C_{Lmax}, an inverse design methodology is employed for this analysis. It is noted that in future design processes this assumption will have to be revisited, when more information about wings and high-lift devices are available. The calculated C_{Lmax} required by the aircraft was 1.017. The Reynolds number for landing was calculated to be in the range of 1148500.

Since the clean C_{Lmax} of the aircraft wing was less than the C_{Lmax} required by the aircraft, there was a need for high lift devices on the aircraft. The use of a wing strake or a leading edge extension (LEX) helps increase the C_{Lmax}. The LEX helps induce leading edge vortices over the wing, which keeps the airflow over the wing from separating and hence leading to a delayed stall. This effect of delaying the stall is illustrated by Figure 16, which also shows the induced vortices over the top surface of the wing because of the LEX.

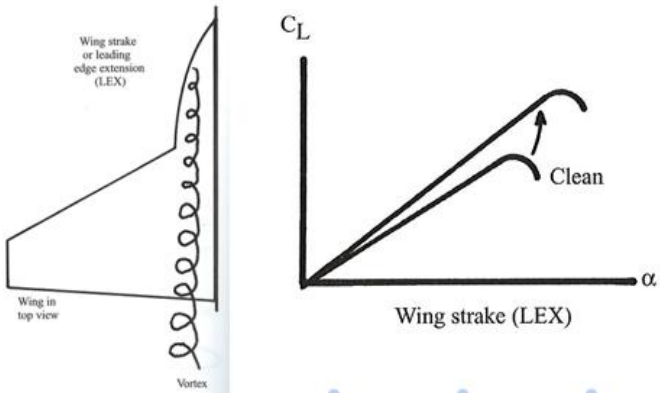

Figure 16: Effect of LEX, Raymer [1]

Extending slotted fowler flaps were also chosen because of the increase in the lift curve slope in addition to the increase in the $C_{Lmax.}$ However, this reduced the stall angle of the wing. The lift coefficient increment given by the addition of the slotted fowler flaps is given by

$$\Delta C_{l\max(slotted-fowler)} = 1.3c'/c$$

Equation 13

$$\Delta C_{L_{\max}} = 0.9\Delta C_{\ell_{\max}} \left(\frac{S_{\text{flapped}}}{S_{\text{ref}}}\right) \cos \Lambda_{\text{H.L.}}$$

Equation 14

where $\Lambda_{H.L.}$is the sweep angle of the mean hinge line of the flap. The ΔC_{Lmax} for takeoff is approximately 60%-80% of the ΔC_{Lmax} calculated for landing from the above equation. In order

to account for the worst case scenario, for the minimum extension of the flap, ΔC_{Lmax} for takeoff was assumed to be 60% of the ΔC_{Lmax} for landing. The effect of using slotted fowler flaps is described by Figure 17.

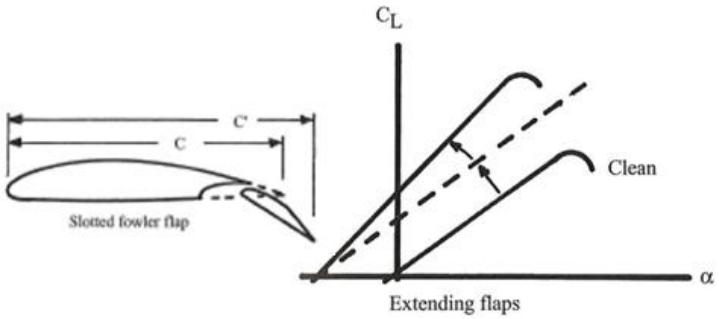

Figure 17: Effect of Fowler flap, Raymer [1]

The size of the flaps required for the aircraft was determined by calculating the minimum extension of the flap required to meet the required C_{Lmax} at takeoff for the wing. A flap span of 40'(full span) was assumed and it was extended over a range of angles of attack. With the use of flaps as well as LEX, it was difficult to analytically determine a stall angle of attack. For this reason, it was ensured that the takeoff C_{Lmax} stayed above the required C_{Lmax} for a range of angles of attack (8˚-14˚). The flapped area on a wing is the part of the wing planform that is projected in front of the flap. For the Supersonix aircraft, the flapped area was 1868.12 sq. ft. Figure 18 shows the flapped area in more detail.

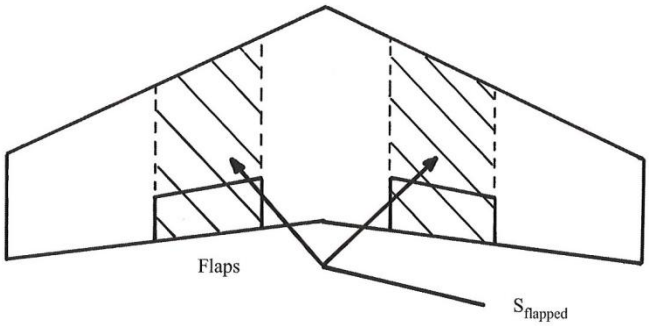

Figure 18: Flapped area, Raymer [1]

Figure 19 shows the C_L vs. angle of attack plots for takeoff and landing along with the required C_{Lmax} as the baseline. At the clean configuration stall angle of 12˚, the take off C_{Lmax} for the worst case scenario is higher than 1.2 times the required C_{Lmax}

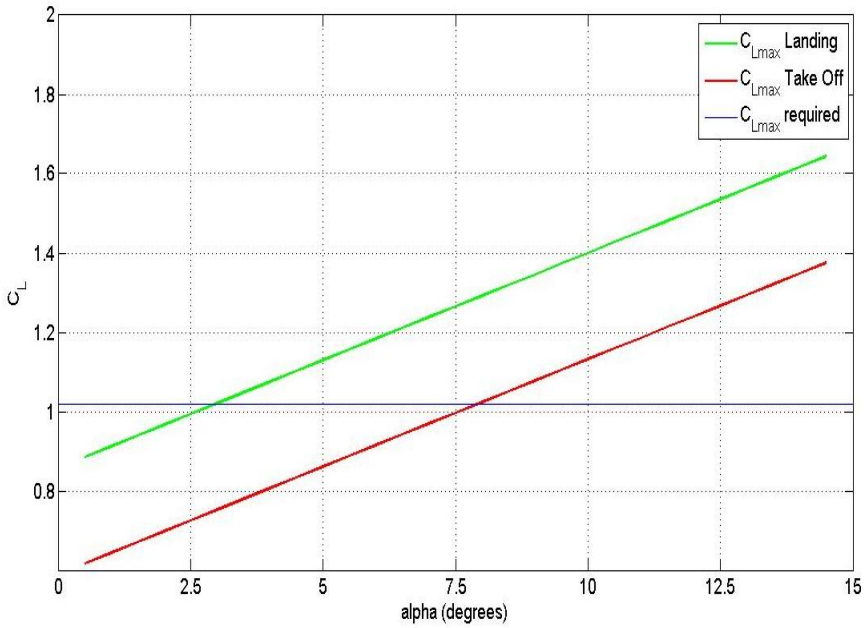

Figure 19: Lift curve using high-lift devices

Drag Buildup

Table 6 shows the breakdown of the drag coefficient for various flight scenarios. This was calculated using the drag code and the details on the calculation involved for each drag coefficient value is explained earlier in the report. The table shows the total drag coefficient C_D and its components – parasite drag (skin friction drag, wave drag and miscellaneous) and induced drag. The different flight scenarios in consideration were

1. Supersonic Cruise (M=1.8, Altitude=60000ft)
2. Subsonic Flight (V=250kts, Altitude=10000ft)
3. Landing (V=170kts, Altitude=10000-0ft)

Each flight scenario had a different value for its C_D. During supersonic cruise, the wave drag has a high effect on the total drag of the aircraft. Wave drag is not present in subsonic flight. 2-D flow effects are predominant in supersonic flight which results in low skin friction component. Induced drag effect is very high during subsonic flight. This is especially true during landing approach where the induced drag component is very high. This is because the induced drag coefficient is proportional to the square of the lift coefficient which is high during landing. As a result, the drag on the aircraft during landing is very high. This value of the drag coefficient would increase when flap deflection during landing approach is taken into consideration.

	C_D	$C_{D,P}$	$C_f+C_{D,misc}$	$C_{D,W}$	$C_{D,i}$
Supersonic cruise	0.06865	0.05890	0.00907	0.04984	0.00974
Subsonic cruise	0.03396	0.01195	0.01195	---	0.02201
Landing	0.2522	0.01195	0.01195	---	0.24025

Table 6: Drag buildup breakdown

The drag polars for the three different flight conditions are shown in Figure 20. For the supersonic flight case and the subsonic case at 10000 ft, the drag coefficient varies over the lift coefficient range. Since the values of lift coefficient in these two operating scenarios are low, its effect on the drag coefficient is not very high. In the landing configuration, due to aircraft operation in the higher lift coefficient range the induced drag effects take predominance and the drag coefficient values are very high. The relation between lift coefficient and induced drag is the reason why the curve looks like a quadratic function.

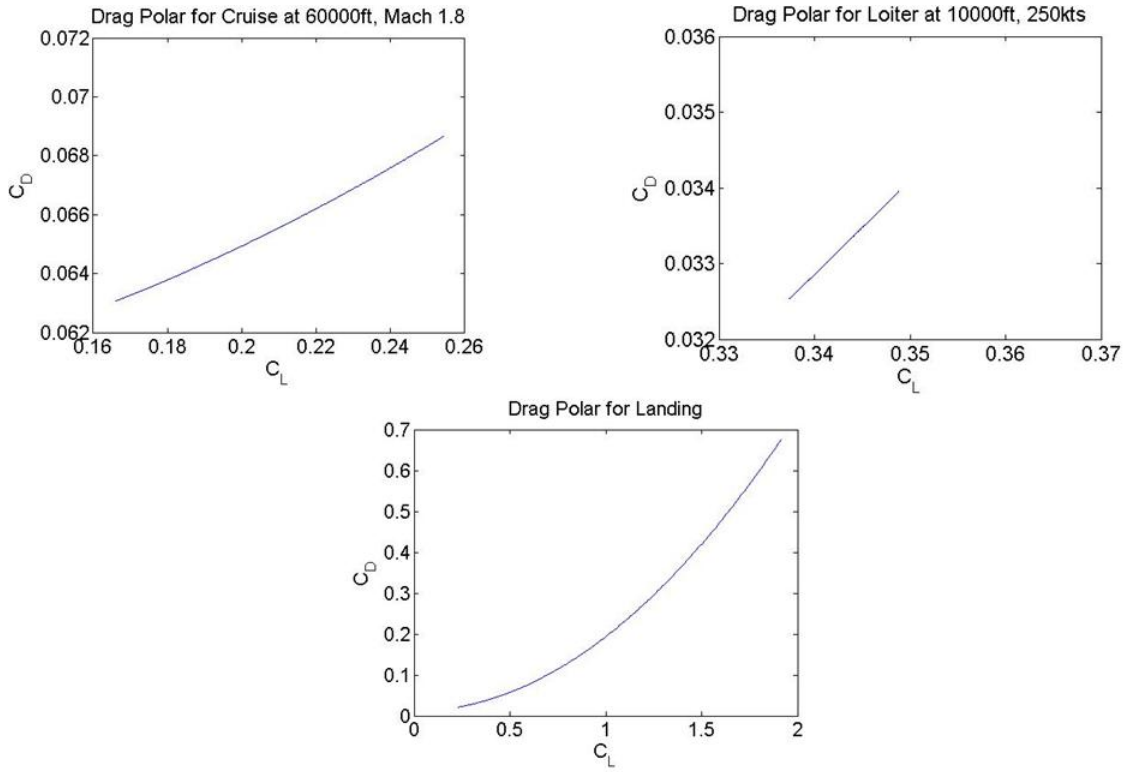

Figure 20: Drag polars for various phases of flight

The lift to drag ratio (L/D) was plotted against the lift coefficient and this is given in Figure 21. In the supersonic flight condition, the L/D value ranges between 2.8 and 3.6 for a range of cruise C_L values. Compared to the Concorde which had an L/D value of approximately twice this

amount, the Supersonix aircraft is a little inefficient in this regard. Detailed analysis into better airfoils and better aerodynamic shaping for the aircraft can change help increase the L/D value at supersonic cruise speed. At subsonic loiter, the aircraft has a much higher L/D reaching values of 10.36. As the aircraft comes in for landing, this high value of L/D decreases due to the increase of C_L which results in the increase of induced drag on the aircraft. This value of L/D will decrease further with detailed analysis where the effects of flaps are considered.

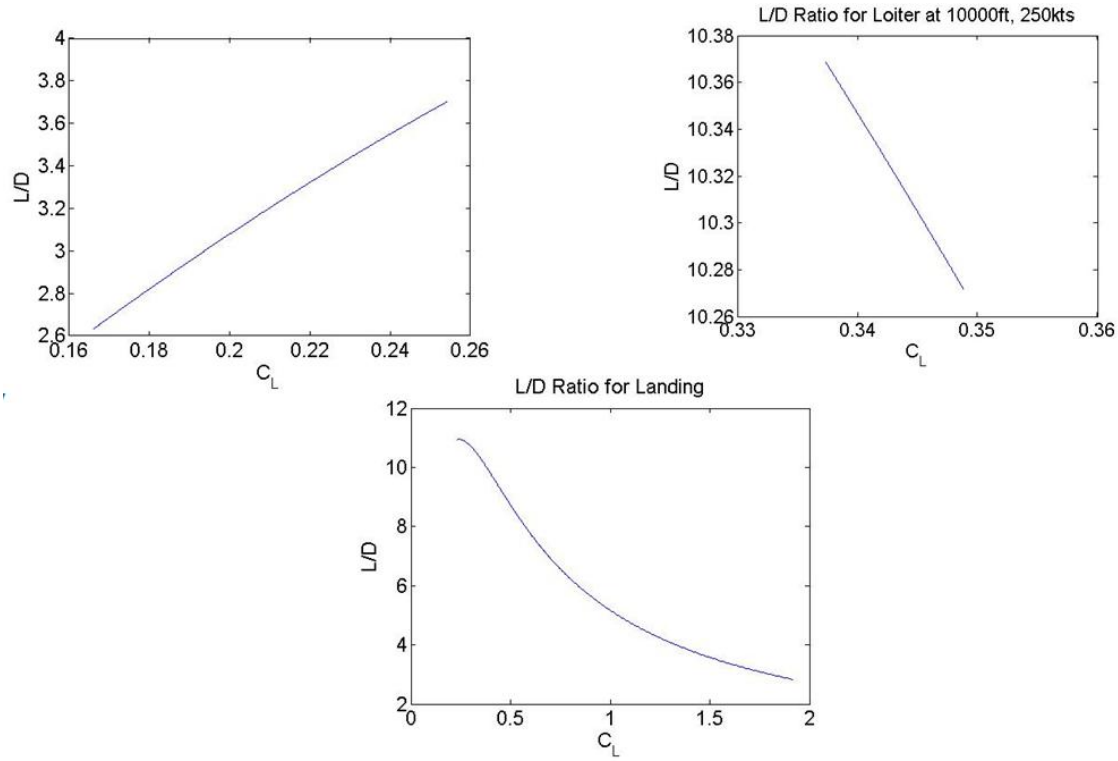

Figure 21: L/D Ratios for various phases of flight

Sonic Boom

The 0.3 lbs/sq.ft overpressure limit is one of the primary reasons why supersonic aircraft are not in operation in the commercial market today. In order for the Supersonix aircraft to get its passengers to the destination fast, it has to surpass this upper limit on overpressure. A number of different technologies were employed to help reduce the sonic overpressure of this aircraft.

1. Blunt nose – The blunt nose design on the Supersonix aircraft will create a bow shock in front of the aircraft which keeps the shock waves from coalescing under the aircraft. This coalescence of shockwaves is the reason for high sonic boom overpressures. They create N-wave shock signatures as in the case of most earlier supersonic aircraft. A blunt nose design will help bring the N-wave shock signature to a plateau wave signature with

a lower sonic overpressure. Conversely, using a blunt nose increases the wave drag of the aircraft. Optimizing the aerodynamic shaping can reduce the wave drag of the aircraft. Figure 22 shows the different sonic overpressure signatures discussed.

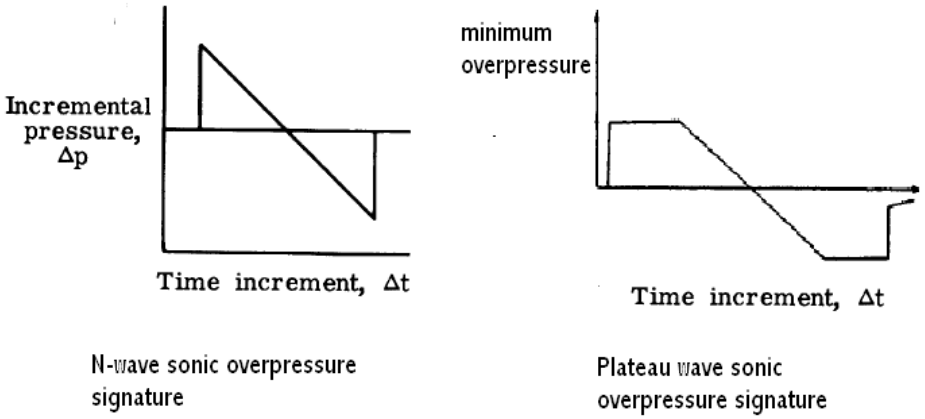

Figure 22: Sonic Boom overpressure Signatures

2. Dihedral angle – A dihedral angle on the lifting surface of the aircraft can reduce the sonic overpressure by making the area distribution smoother, which has a high effect on the sonic overpressure signature. Also, a dihedral angle has the effect of increasing the effective length of the aircraft.
3. Low AR, high sweep – A high aspect ratio, low sweep wing has the effect of increasing lift rapidly over the wing. This is another major reason for the creation of N-wave shaped sonic signature. A low aspect ratio, highly swept wing brings the aircraft sonic boom overpressure signature to that of a plateau wave.
4. Smooth area distribution – A smooth area distribution is vital to reduce creating multiple shocks at multiple locations on the aircraft. Smooth area distribution coupled with the blunt nose design will help bring down the chances of multiple shocks originating all over the surface of the aircraft, which could coalesce together to give a high sonic overpressure.

Two different techniques were employed to calculate the sonic overpressure on the aircraft. One technique was based on the "Simplified sonic boom prediction" paper by Harry W. Carlson. The other method used was developed by R. Seebass and A.R. George in the paper titled "Sonic-boom minimization"[3]. While the Carlson method makes use of the area distribution of the aircraft to determine the shape factor of the aircraft and use the shape factor to calculate the N-wave overpressure signature, the Seebass method makes use of basic aircraft parameters (Weight, length, Mach number, etc…) to determine the plateau overpressure signature of the aircraft.

From the preliminary sonic boom analysis on the Supersonix aircraft, the following results were obtained, as shown in Table 7. The Carlson method was calibrated using the sonic overpressure from the F-5 sonic boom demonstrator and the correction factor was found to be 1.09. The Seebass method had a higher correction factor, but this can be attributed to the shape/size of the F-5 demonstrator- the short length of the aircraft has a detrimental effect on the Seebass method calculation. In earlier computations using simplified area distributions, the Carlson method gave a higher sonic overpressure value when compared to that calculated using the Seebass method. This made sense because the peak (N-wave) overpressure signature had a higher value when compared to the plateau wave signature. For this reason, the Carlson method overpressure was taken as the upper bound and the Seebass method overpressure was used as the lower bound for over pressure calculation. However, when the area distribution of the Supersonix aircraft was optimized to give the best value of over pressure using the Carlson method, a low overpressure value of 0.28psf was obtained. The overpressure from the Seebass method had a much higher value which could be attributed to the disadvantage of the method in not using the area distribution of the aircraft and just relying on basic aircraft parameters.

Method	Overpressure (lb/sq. ft)
Carlson	0.28
Seebass	0.71

Signature Duration, Δt	0.03s

Table 7: Seebass and Carlson Overpressures and duration

Since the Carlson method was used to calculate the aircraft sonic overpressure based on the aircraft geometry, it is chosen as the more reliable of the two methods and is explained in more detail. The Carlson method was obtained from NASA Technical Paper 1122 titled "Simplified Sonic-Boom Prediction"[2]. Although this method gives a rough estimate of the sonic overpressure and signature duration, much more research and analysis in supersonic sonic boom mitigation is required to develop the final aircraft design. The Carlson method involves three major steps to calculate the sonic boom overpressure and its time signature.

1. Determine Shape factor – In order to calculate the shape factor of the aircraft,

    a. Generate axis normal cross-sectional area distribution – The cross-sectional area distribution along the length of the aircraft was generated by the A/C Geometry function in the sizing code. Details about this process were discussed earlier in the aircraft geometry section. The wireframe area

distribution is shown in Figure 23 along with the area distribution for the aircraft geometry.

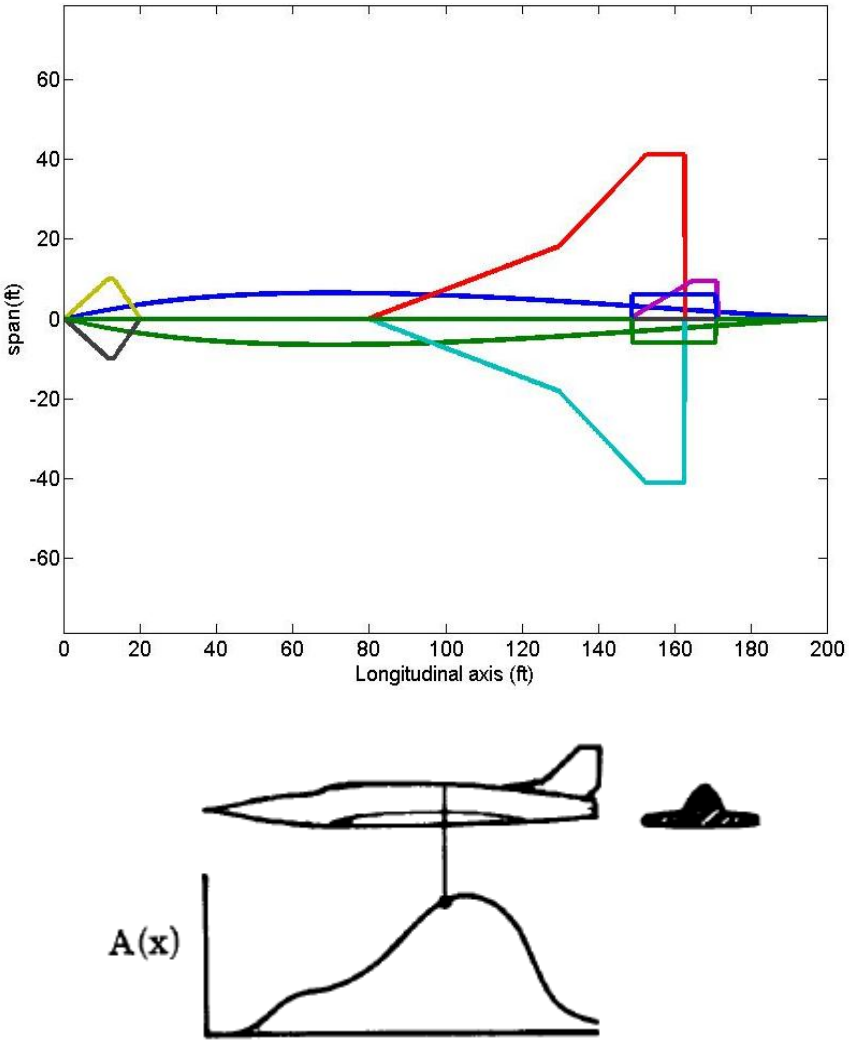

Figure 23: Aircraft Wireframe area distribution

(image courtesy: Carlson [2])

b. Equivalent area due to lift – A reasonably accurate approximation of the equivalent area due to lift is calculated from the span distribution along the length of the aircraft. This has been described in Figure 24, where b(x) is the span wise distribution along the length of the aircraft. This is used to calculate the equivalent area distribution, B(x). B(x) is calculated using the equation

$$B(x) = \frac{\sqrt{M^2 - 1}\ W \cos\gamma \cos\theta}{1.4 p_v M^2 S} \int_0^x b(x)\ dx$$

Equation 15

where M is the supersonic cruise Mach number of the aircraft, p_v is the atmospheric pressure at vehicle altitude, W is the weight of the aircraft, S is the planform area, γ is the flight path angle (0˚ for steady- level flight) and θ is the initial ray path angle (0˚ if directly under flight path). *(image courtesy: Carlson [2])*

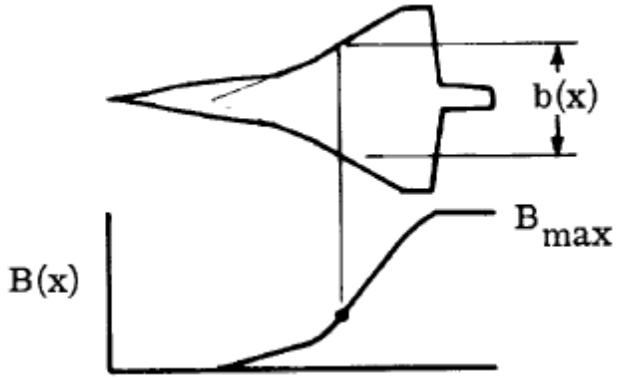

Figure 24: Span distribution and effective area

c. Combined effective area – The geometric area combined with the equivalent area due to lift gives the effective area. The combined effective area for the Supersonix aircraft is given in Figure 25. This distribution curve was smoothened to yield a better plot with lesser kinks.

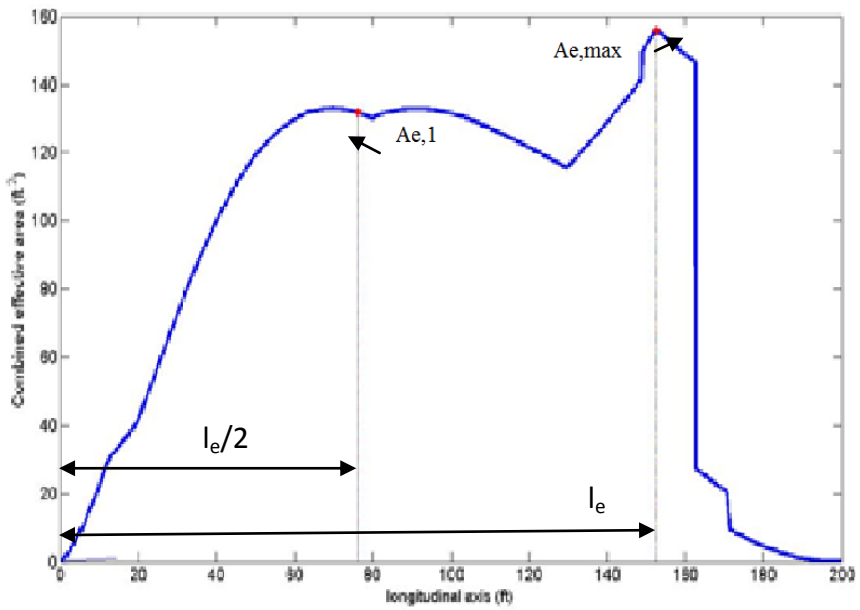

Figure 25: Supersonix Effective area distribution

Using the values obtained from Figure 25 and the chart in Figure 26 *(image courtesy: Carlson[2])* the value of the shape factor was calculated.

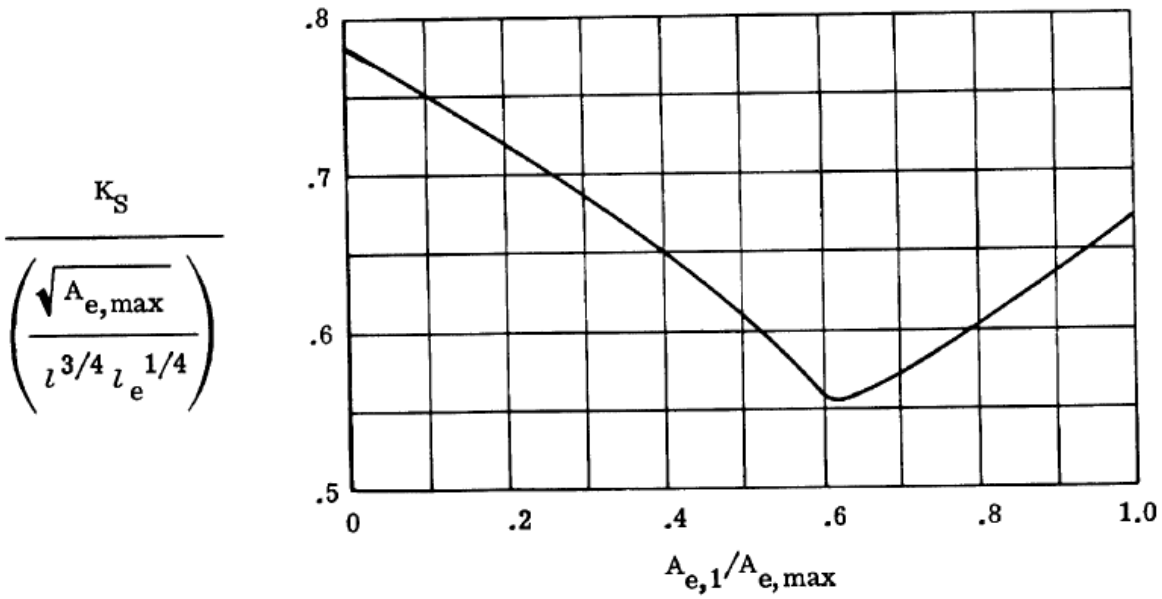

Figure 26: Shape factor as a function of effective area parameters

2. Calculate effect of atmosphere on propagation – The effect of atmosphere on boom propagation needed to be calculated. This was done by determining the effective Mach

number and effective altitude of supersonic cruise. The effective Mach number is given by the formula (Carlson)

$$M_e = \sqrt{1 + \frac{[A(1 - B\tan\gamma)]^2}{[A(\tan\gamma + B)]^2 + (CD)^2}}$$

Equation 16

$$A = \frac{1}{\cos\gamma\sqrt{M^2 - 1}}$$

$$B = \frac{1}{\cos\theta\sqrt{M^2 - 1}}$$

$$C = \frac{\tan\theta}{\sqrt{M^2 - 1}}$$

$$D = \tan^2\gamma + 1$$

The effective altitude is calculated using the formula

$$h_e = \sqrt{d_y^2 + [(h_v - h_g)\cos\gamma + d_x \sin\gamma]^2}$$

Equation 17

where,

$$K_d = K_{d,c} + (K_{d,\infty} - K_{d,c})\left(\frac{M_e - M_c}{M_e - 1}\right)^{n_d}$$

$$K_p = K_{p,\infty}\left(\frac{M_e - 1}{M_e - M_c}\right)^{n_p}$$

$$K_t = K_{t,\infty}\left(\frac{M}{M - 1}\right)^{n_t}$$

$$d = \frac{K_d(h_v - h_g)}{\sqrt{M_e^2 - 1}}$$

$$d_x = d\cos\phi$$

$$d_y = d\sin\phi$$

3. Calculate bow shock and time signature – The peak shock overpressure, ΔP is calculated using the following formula (Carlson)

$$\Delta p_{max} = K_p K_R \sqrt{p_v p_g}\,(M^2 - 1)^{1/8} h_e^{-3/4} \ell^{3/4} K_S$$

Equation 18

The signature duration is given by Δt,

$$\Delta t = K_t \frac{3.42}{a_v} \frac{M}{(M^2 - 1)^{3/8}} h_e^{1/4} \ell^{3/4} K_S$$

Equation 19

Performance

V-N Diagram

The Supersonix aircraft is designed to provide time and money savings in long distance travel. For safety design purposes a V-N Diagram must be created. The V-N diagram looks at an aircraft's loading factor as a function of velocity and design mission requirements (2g and -1g maneuvers). The gust diagram is superimposed onto the V-N diagram. The maximum positive load factor is 3.72 at 742knot, while the maximum negative load factor is -1.72 at 742knot. Different velocities that are marked by the vertical lines are the 2g maneuver, maximum gust intensity design speed $V_{b,}$, design cruise speed V_c, and design dive speed V_d. The gust diagram shows the gusts that the aircraft might experience flying at specific altitudes. The outer limits of the V-N and gust diagram must be taken.

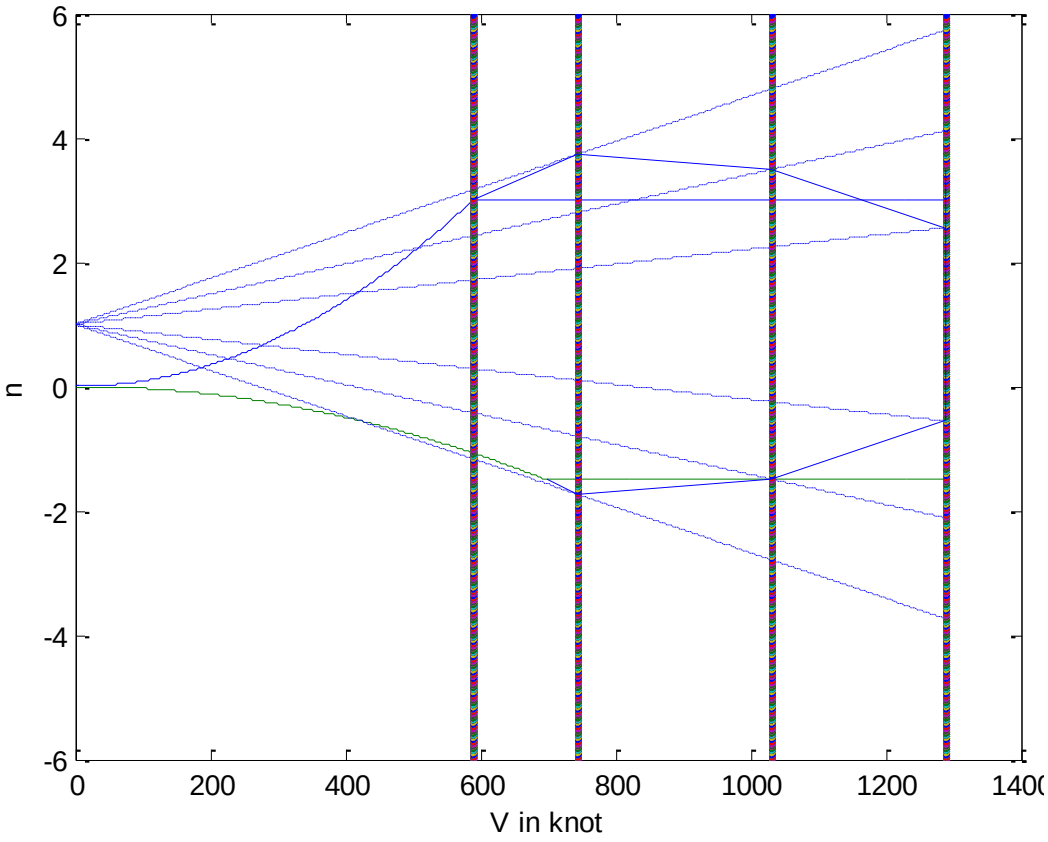

Figure 27: V-N Diagram

Velocity (knots)	590	742	1032.3	1290.3
Maximum Positive Loading factor	2.5	3.72	3.49	3
Maximum Negative Loading factor	-1.5	-1.72	-1.49	-0.56

Table 8: Load factors from V-N Diagram

Range Diagram

Creation of the range diagram provides an outline for cargo loading capability of the aircraft with corresponding range. The numerical values were derived from the Breguet's range equation from the start of cruise to the end of cruise. The initial aircraft weight with fuel weight has to correspond to the mission statement at the beginning of cruise end of climb. The maximum zero range for this aircraft is the maximum cargo load. There is no horizontal steady range for the Supersonix aircraft because of the aircraft's fuel requirements. The Supersonix aircraft cannot reach its operational altitude with a cargo weight equal to the amount of fuel. The aircraft range at MTOW is 4153 nm, with the maximum range (ferry range of 4882 nm. Figure 28 below shows tradeoff between fuel and cargo. After the intersection point, the aircraft trades cargo weight for fuel weight. All ranges presented are cruise ranges only.

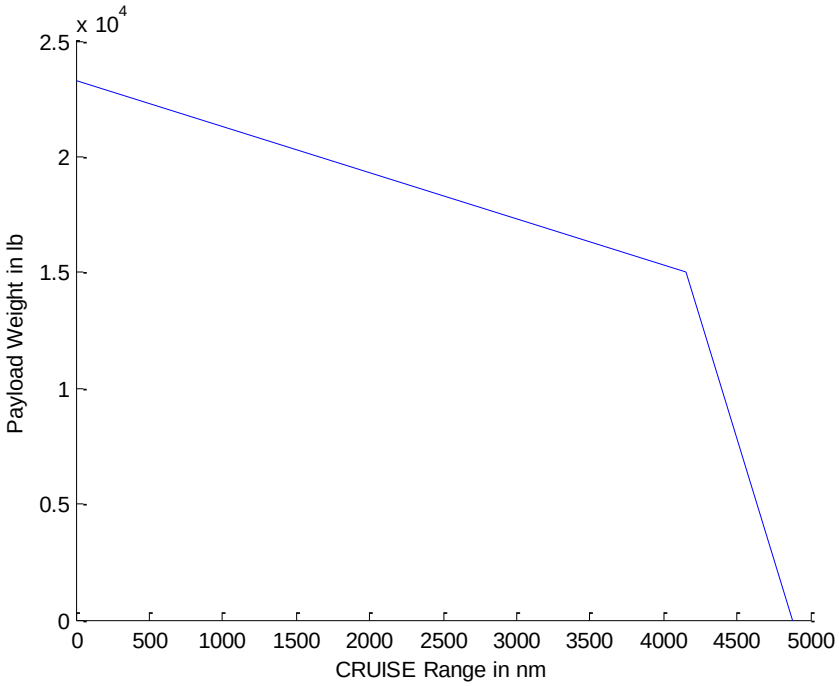

Figure 28: Payload-Range diagram

Propulsion

Inlet

The engine performance is crucial if the Supersonix aircraft is to achieve its mission. The inlet is the first design consideration for the engine. The inlet is important because it affects vital performance parameters such as fuel consumption and thrust. According to Raymer[1] (Chapter

10 pp 228), a 1% decrease in the pressure recovered from the inlet will result in a 1.3% decrease in installed engine thrust.

There are 4 types of inlets. The NACA flush inlet is mostly used on engines where pressure recovery is not as important. The Normal shock inlet has been found to be desirable at subsonic speeds because it has 100% pressure recovery (theoretically).

Spike inlets and Ramp inlet are the two remaining types of inlets, both of which are suitable for supersonic speeds. The Spike inlet is lighter and has better pressure recovery; however it has higher cowl drag and is more complicated than the 2-D ramp inlet. Spike inlets are typically used in speeds above Mach 2, while ramp inlets work best for speed less than Mach 2. Due to the designed flight envelope of the Supersonix aircraft, the 2-D ramp inlet was chosen.

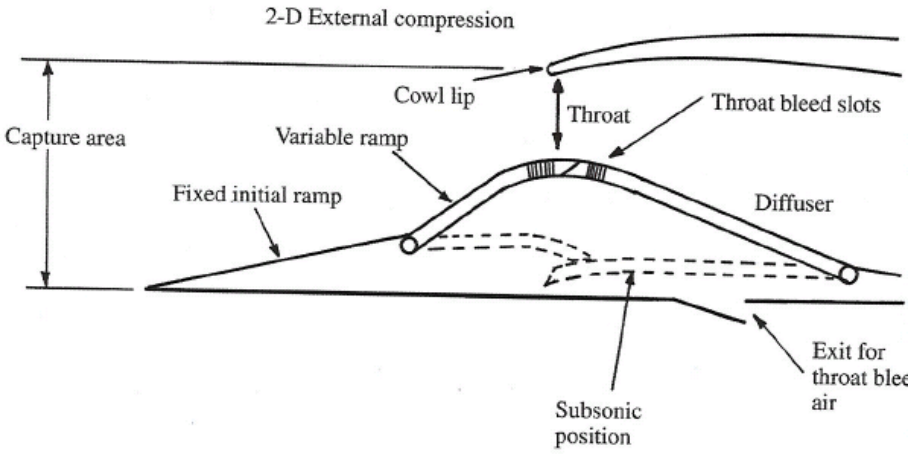

Figure 29: 2-D Ramp Inlet

Figure 29 above shows a side view of a three-shock external compression inlet from Raymer[1] (Chapter 10 pp 232). Using the σ-δ-M relationship, the initial ramp angle is found to be 15 degrees. The engine must have a pressure recovery of 95% for efficient flight at Mach 1.8. However, the σ-δ-M figure does not show detailed lines for cruise speeds below Mach 1.5. Therefore, the ramp angle was unobtainable for the remaining ramps given the available information.

The Supersonix aircraft will have variable ramps which can help during subsonic flight. Variable ramps are necessary for the Supersonix aircraft because of its need to be able to fly in both subsonic and supersonic conditions efficiently. The Concorde has two intake ramps and one auxiliary inlet. The variable ramps are designed to fully open during take-off and subsonic cruise in order to take in as much air as possible.

Engine Description

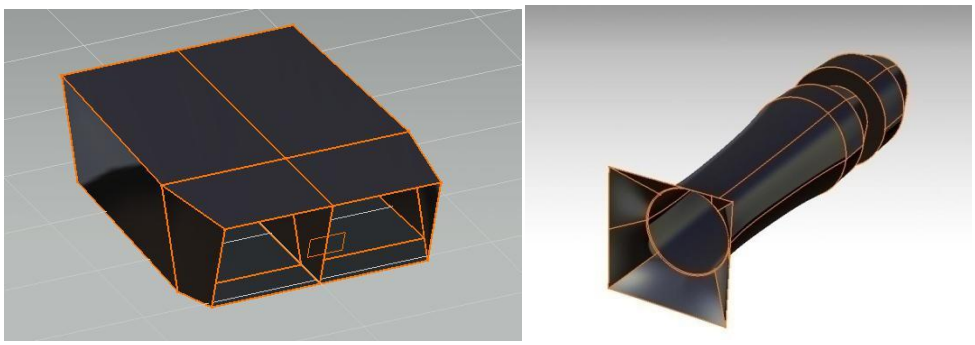

Figure 30: CAD engine models

The figures above are the CAD model of the Supersonix Engine.

The Supersonix engine is a low Bypass Turbofan with an afterburner. It produces 38,500 pounds of thrust (per engine) and it weighs 3000 lbs. Table 8 below gives the engine specification.

BPR	1.627
Fan Ratio	4.3
Area	41 ft^2
Diameter	7.2 ft
Length	33 ft

Table 9: Engine specification

The calculation for the engine performance was found from the sizing code, and the dimensions were found using Raymer[1] (Appendix E) and ONX-OFFX.

Nozzle Design

Figure 31 shows eight types of nozzles from Raymer (Chapter 10 pp 248). The four on top are mostly used in subsonic aircraft. 2-D vectoring is only used by fighter jets and the Single Expansion Ramp is used only in scramjets. Currently only converging-diverging nozzles are commonly used for supersonic aircraft and this is the only viable option for Supersonix Nozzle.

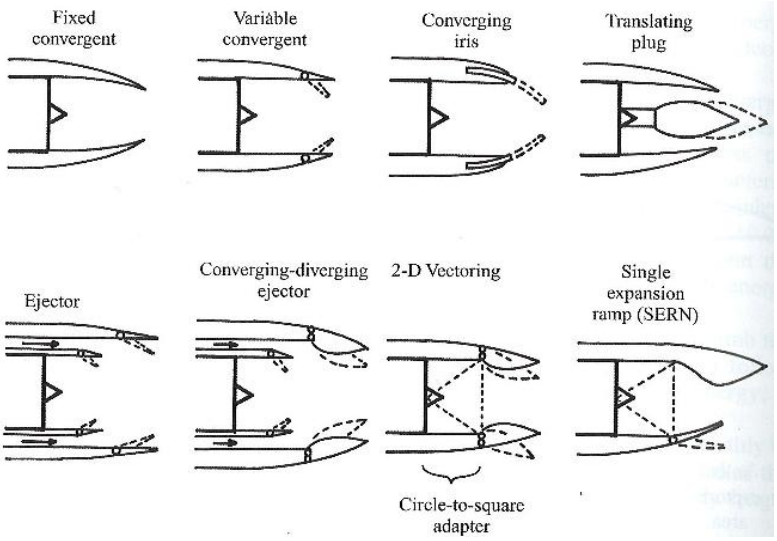

Figure 31: Types of Nozzles. (Raymer[1])

Converging-diverging nozzles allow the exit area to vary to maintain maximum engine performance. In a converging-diverging nozzle exhaust from the combustor converges to the throat. The throat is needed to choke the flow, which determines the mass flow rate. The throat area has to be chosen to produce Mach 1 at the throat. The flow then diverges and is expanded isentropically to a supersonic speed. The exit area determines the exit speed and this can be calculated as a function of the ratio between throat area and exit area. By increasing the mass flow and the exit speed from this nozzle design, more thrust is produced.

Another possible future technology is the mobile chevron exhaust nozzle[7] A Chevron exhaust nozzle is a nozzle in which its extreme ends have non-smooth shaping. This is done most frequently on aircraft to reduce the noise. Many aircraft are currently using the fixed chevron nozzle; however, Chevrons do have disadvantages. Chevrons actually reduce nozzle efficiency. A turbofan with Chevron will also use more fuel than the one with a normal smooth nozzle.

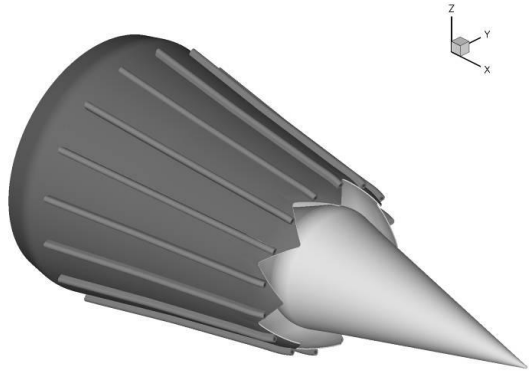

Figure 32: Fixed Chevron Nozzle [7]

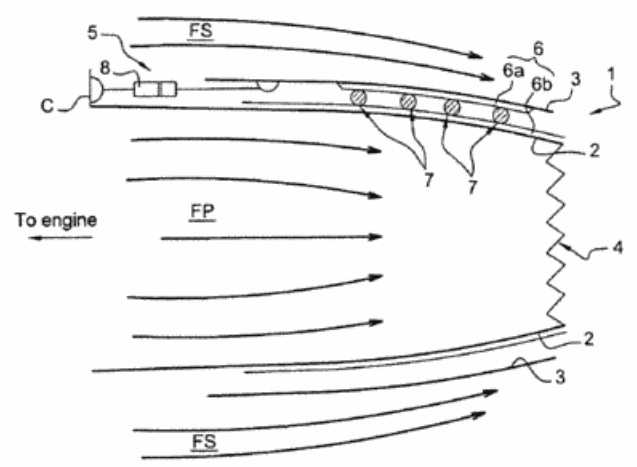

Figure 33: Mobile Chevron Nozzle[7]

Adding Chevrons can increase thrust in a low speed flight. However, presence of Chevrons reduces the thrust in a high speed flight regime. This invention claimed that sliding Chevrons could be produced so that both the benefits of a smooth nozzle during high speed and the benefits of Chevrons during low speed flight could be obtained.

Double coating the nozzle was also proposed (one for cold air and one for hot air), so that the outer coat is interchangeable with the inner one. The nozzle would have the benefits of Chevrons at low speed, take off and landing, but would also maintain a smooth nozzle benefit for the rest of the flight mission.

Details of this invention are very limited, but fixed Chevrons have been used before and hopefully this invention can be implemented by 2020.

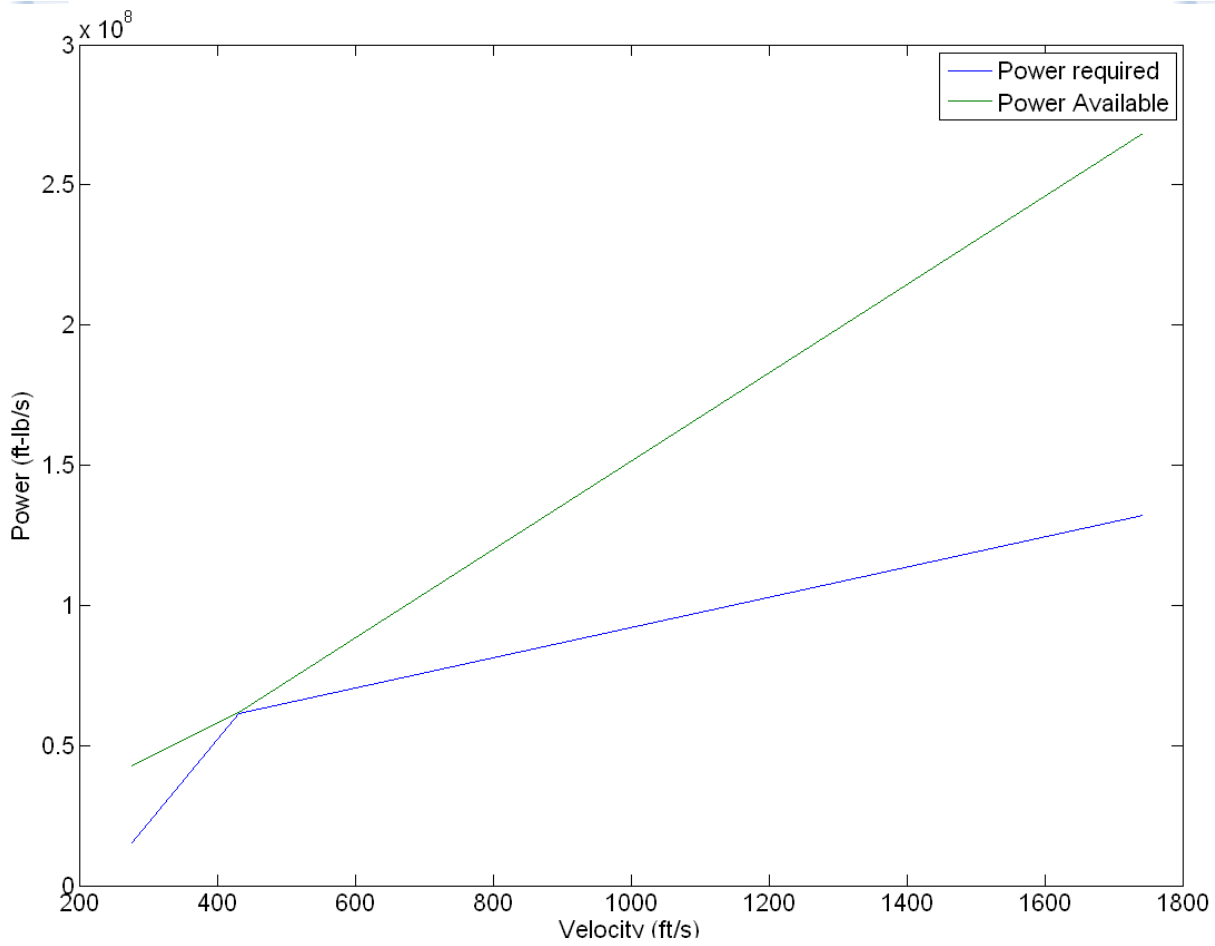

Figure 34: Power required and Power available VS Velocity

The plot above depicts the power required and available versus airspeed. The starting point is at take off speed. The point where the two lines almost intersect is the 2-g maneuver, which sets the carpet plot constraint. The final point in the plot is at a cruise speed, where there is ample excess power.

Structures

The lift force acting on the aircraft is assumed to be equal to twice the maximum takeoff weight of the aircraft, which is 616000 lb. This is due to the aircraft design load at n=2. The top plot in Figure 35 shows the top down view of the wing and location of the quarter chord. The 2nd and 3rd plots show the bending moment and lift force acting on the wing.

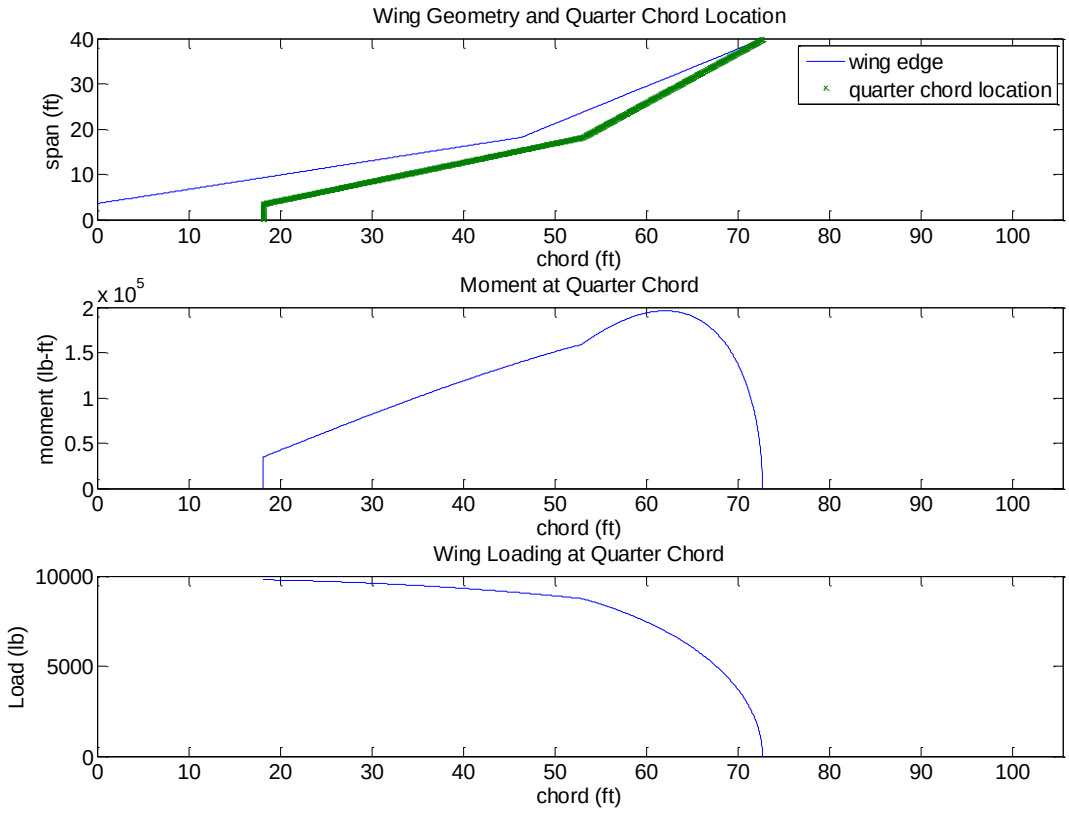

Figure 35: Wing loads

Based on our design load and the requirement stated in FAR section 23.303,("Safety factor of 1.5 must be applied to the prescribe limit load which are considered external loads on the structure"), our aircraft wings must be able to withstand 924000 lb of lift. From this analysis, we have decided that for the wing to be able to resist the bending moment due to lift, 5 spars needed to be installed in each wing as shown inFigure 36. The 3rd and 4th spars are installed near to each other because that particular area on the wing produces high bending moment. Putting 2 spars at that location distributes the high bending moment and each spar doesn't have to carry excessively high bending moment. Furthermore, the spars will also provide rigidity to the wings. Our aircraft wing ribs are forming the structure of the wing and they incorporate the wings' airfoil shape. The ribs sizing will need to be determined in the future as this analysis is not done at this stage. As for now, our aircraft ribs are spaced 2 feet apart, which is the average spacing distance in most aircraft[16]. The exact spacing can be determined by analyzing the skin panel buckling. However, this analysis has not been performed because of its complexity.

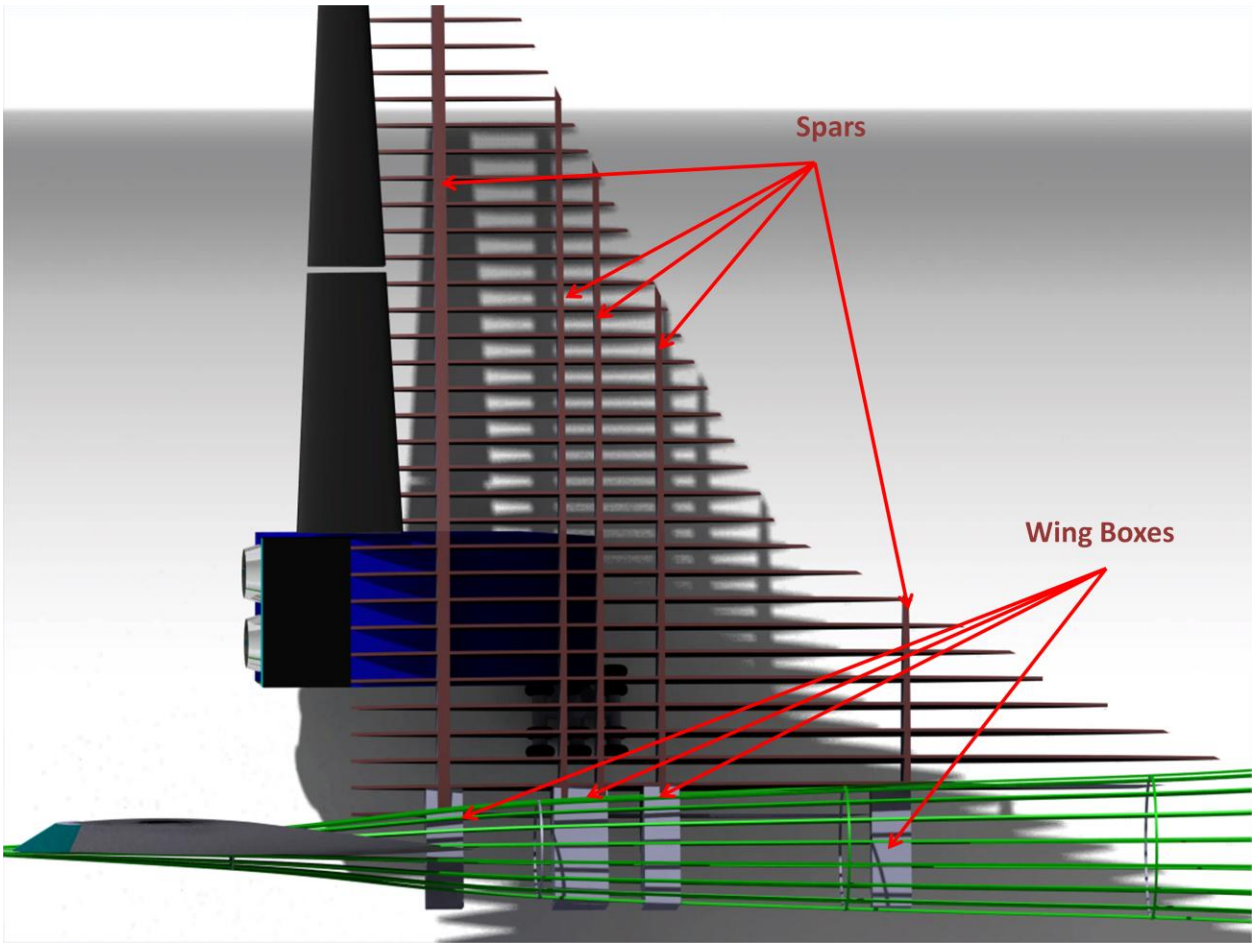

Figure 36: Wing structural elements

In fuselage construction, we use stringers to carry fuselage load and to prevent bending. The stringers are bonded to the co-cured composite skin around the circumference of the fuselage. The used of co-cured skin will be discussed in later part of this report. The stringers are aligned as straight as possible so the weight can be minimized (Raymer[1] Chapter 8). At this stage, further analysis need to be conducted in order to determine the exact number of stringers needed in the fuselage construction. For the carry through structure, we have chosen "box carry through" as depicted in Figure 36. This configuration is standard for high speed transports and the configuration provides the minimum weight (Raymer[1] Chapter 8). The wing boxes are positioned under the cabin deck. Our aircraft will also employ semi-monocoque composite skin structure to help bear the load in the wings and fuselage. Semi-monocoque fuselage can bear considerable amount of damage and still remain strong to hold together [9].

Engine mounting

Our aircraft will have four engines, two under each wing, and mounted on the 4th and 5th spars. This will ease the maintenance and optimize span loading effect to help in lift (Raymer[1] Chapter 8). They are located at the back, away from the cabin for safety reasons.

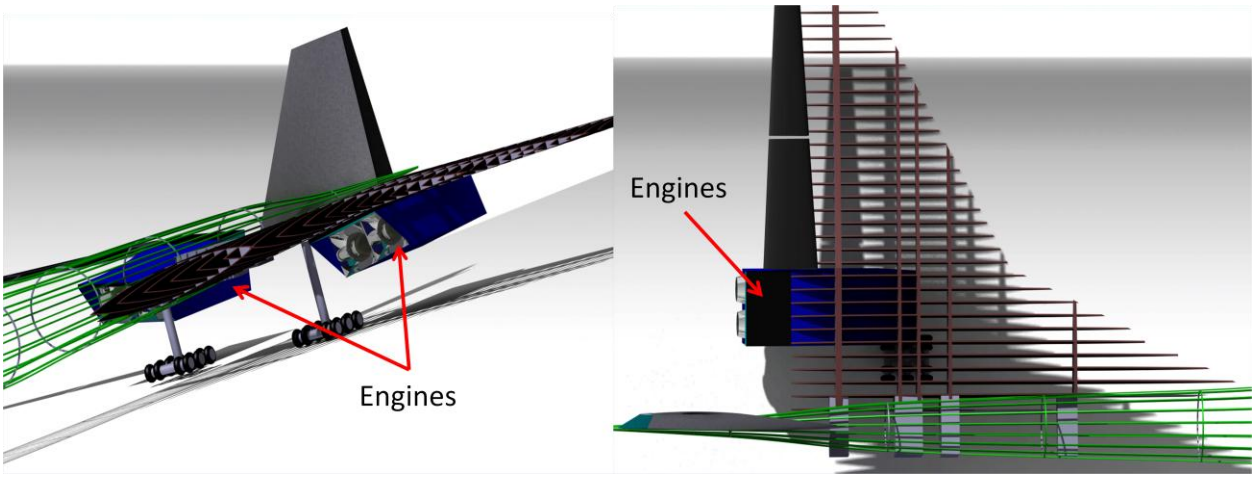

Figure 37: Engine mounts structure

Landing gear

Landing gear placement is important as it will affect the stability of the aircraft on the ground. Using the principle of conservation of energy and static equilibrium, we have determined that our aircraft main landing gear will be located 120 ft from the nose, between 4th and 5th spars, which will be our landing gear bay. Please refer to Figure 38for the landing gear view. It is designed with safety factor of 3, which is common for general aviation aircraft (Raymer[1] Chapter 8). Our aircraft main landing gear will carry 90% of the aircraft weight. The landing gear has to be able to withstand 1904580 lb force during landing (assuming a 2-g hard landing) and 833488 lb force during taxi. For nose landing gear, it is located 55 ft from the nose, and also designed with safety factor of 3. The nose landing gear will carry 10% of the aircraft weight. This percentage is important because nose gear has to carry 8-15% of aircraft weight so that it will have enough traction to steer the aircraft (Raymer[1] Chapter 8).

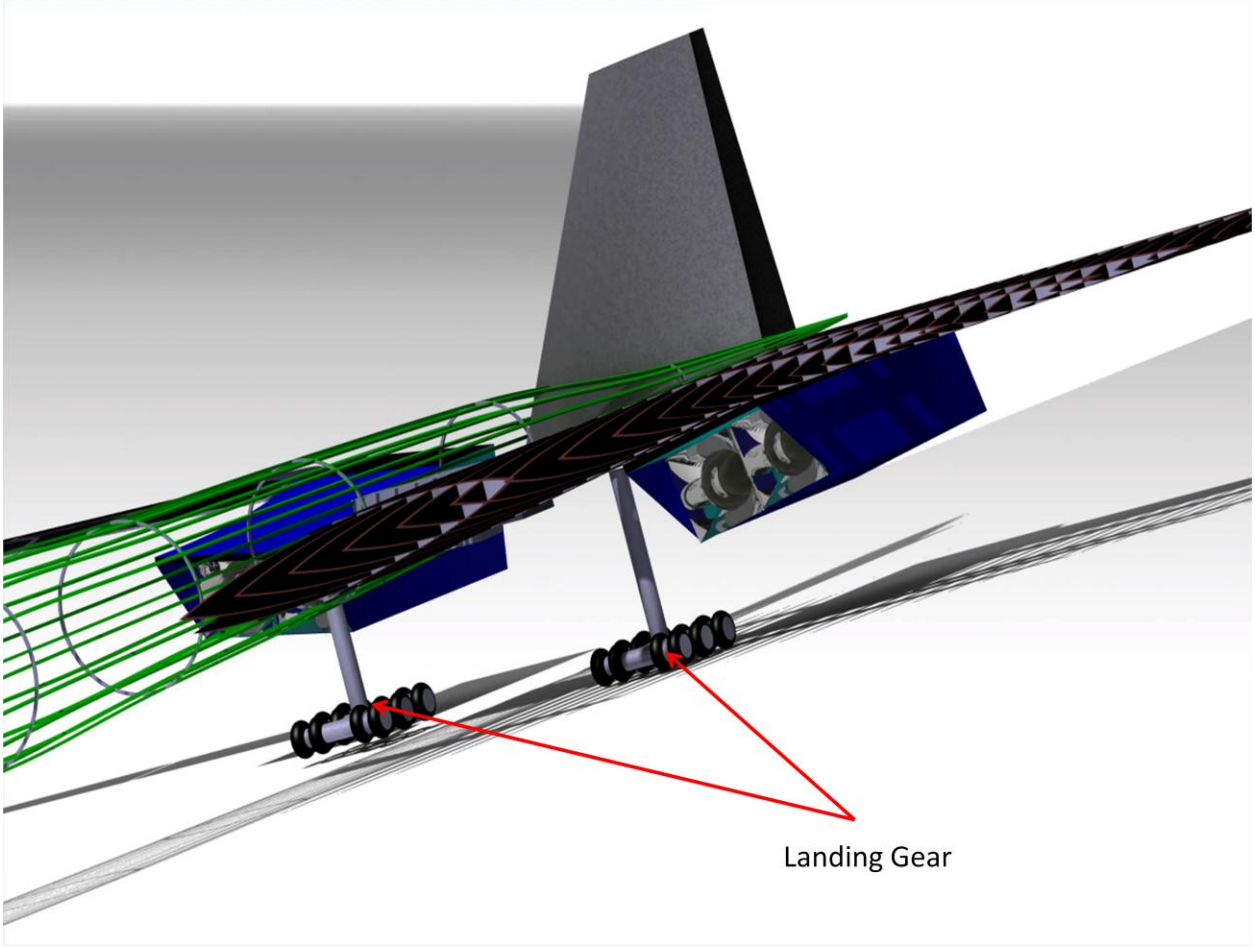

Figure 38: Landing gear structure

Material selection

Proper material selection can reduce the aircraft weight and increase the safety of our aircraft. From our calculation, this aircraft will consist of 70% composites by weight. The value was obtained by taking the component weights of the parts that will be constructed from composites and finding their ratio compared to the aircraft maximum takeoff weight. Fuselage and wings skin will be constructed from graphite/epoxy. Based on Concorde's service temperature, the aircraft skin will experience temperature up to 100°C [10]. Therefore, epoxy is a good choice as it is lighter and has suitable service temperature [15]. In addition, as we are employing semi-monocoque skin, carbon/epoxy can handle high load and serves the purpose. The nose as well as leading and trailing edges of the wing will be constructed from graphite/polyimide as these parts will experience the highest temperature, which about 130°C [10]. Epoxy is not used as a matrix in these parts because we are concerned about creep failure, although epoxy can withstand the high service temperature. Polyimide is better than epoxy in thermal properties and lighter compare to titanium, which is another material considered for

these parts [8]. Spars, ribs, and stringers will be constructed from carbon/epoxy as well due to the high compressive and yield strength it offers[15].

The landing gear will be constructed from AF-1410 Steel, which is replacing 300M steel as main material in landing gear construction [11]. It has higher corrosion and fatigue resistance than 300M and shows excellent fracture toughness [11]. Titanium was also one of the materials considered, but the price is too expensive[15]. So we chose AF-1410 due to its cheaper price although it is a bit heavier[15].

From all the materials chosen, the weight savings that we can achieve is approximated to be about 20-30% of maximum takeoff weight compared to just using traditional materials such as aluminum [12,13]. The weight saving is not very much due to the mechanical fasteners, which are made of titanium, that will be used to connect the parts together[14]. However, new manufacturing techniques such the usage of co-cured skin, where stiffeners are integrally cured with the skin in one cure cycle, and the usage of polyimide epoxy adhesive such as FM1000, can reduced the number of fasteners used and thus higher weight saving could be obtained [12,17,18].

Weights and Balance

Aircraft Component Weight

An accurate estimate of aircraft empty weight is critical for aircraft design. Database estimates of aircraft component weights varying with internal and external characteristics must be established. The purpose of the aircraft component weight estimate is to create a program that can be iterated with a varying external input. A limited database exists, consisting of the Concorde and the Russian Tu-144. The Concorde was taken as the baseline datum for weight equations.

Estimate equations for component weight are obtained from Raymer[1] (Chapter 15.) Equations for Fighter aircraft and transport aircraft are given with input variables for 98 different aircraft characteristics. The equations selected for individual component parts are based on similarity to the design mission. For example, the selection of the wing equation for the Supersonix is an average of the Fighter and the Transport equations, because of the high Mach number that the Supersonix will travel at, and the large wing surface area (like the transport).

Component weight equations are put into MATLAB as a standalone script, capable of iterating through two main variables and providing an estimated empty weight. Dimensional characteristics of the Concorde are input as the datum. The sum of all total component weights should be equal to the published Concorde empty weight. A correction factor of 1.07 is

necessary as a result of this baseline comparison. To check for validity of component weight trend, a 'test run' mesh plot is created for varying wing aspect ratio and aircraft length.

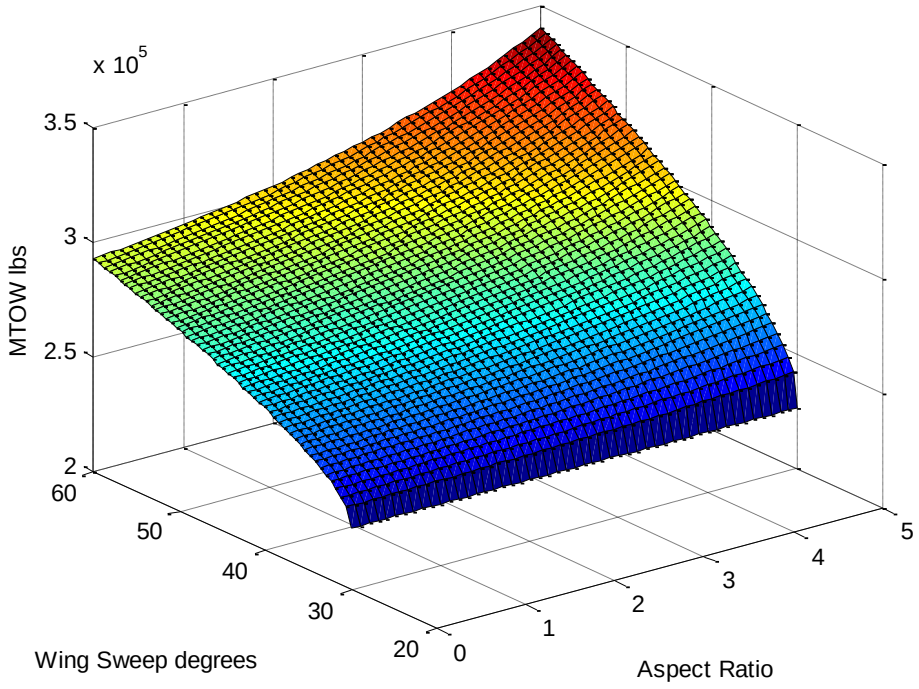

Figure 39: MTOW vs wing sweep and Aspect Ratio

The upward trend-line for the empty weight is expected due to increases in either aspect ratio or aircraft length. The concaved curvature of the mesh plot resembles a capability to be optimized. This mesh plot allows for a component weight code that takes inputs from the geometric iteration and area distribution codes. The outputs of the function are empty weight and component mass fraction. After the design is finalized, an aircraft weight and balance statement is created. This is shown in Table 10 below.

Structures	Weight (lb)	Location (ft)	Mass Fraction (%MTOW)	Moment (ft-lb)
Air Induction	7330.87	128	0.0238	938352.128
Engine Mount	3696.24	166	0.012	613575.84
Canard	733.08	35	0.00238	25658.066
Firewall	28.18	128	0.0000915	3607.53024
Fuselage	17218.31	94	0.0559	1618521.892
Main Landing Gear	7700.5	146	0.025	1124273
Nose Landing Gear	1466.17	30	0.00476	43985.256
Vertical Tail	6591.62	170	0.0214	1120576.76
Wing	53287.46	128	0.173	6820794.88
Total Weight	98052.46		0.3183315	12309345.35

Propulsion	Weight (lb)	Location (ft)	Mass Fraction (%MTOW)	Moment (ft-lb)
Engine	12000	166	0.03896	1992000
Engine Cooling	131.52	166	0.000427	21833.07364
Fuel System/Tanks	2149.97	130	0.00698	279497.348
Total Weight	14281.50		0.046367	2293330.422

Equipment	Weight (lb)	Location (ft)	Mass Fraction (%MTOW)	Moment (ft-lb)
APU	1150	170	0.003733524	195500
Avionics	1466.17	14	0.00476	20526.4528
Air Conditioning/Anti-Ice	545.19	90	0.00177	49067.586
Electrical Systems	5143.93	90	0.0167	462954.06
Flight Control	1004.14	174	0.00326	174721.2648
Furnishing	1352.20	56	0.00439	75723.6368
Hydraulics	253.50	152	0.000823	38532.06992
Handling Gear	84.39	120	0.000274	10127.6976
Instruments	489.75	14	0.00159	6856.5252
Total Weight	10339.30		0.033567	1034009.293

Aircraft Empty Weight	122673.28		0.39	1.56E+07

Table 10: Group Weights Table

Stability and Control

Static Longitudinal Stability

An important condition for maintaining the longitudinal stability of the aircraft is the static margin. The static margin is the difference in length between the center of gravity and the neutral point of the aircraft. If the center of gravity is fore of the neutral point, the aircraft is said to be stable.

The neutral point of an aircraft can be approximated by assuming that it is located at 25% mean aerodynamic chord (MAC) for subsonic flight and 40% MAC for supersonic flight. A slightly more accurate approximation includes a term based on the horizontal tail dimensions (canard dimensions in our case). This results in a neutral point of 25.4% MAC for subsonic flight and 40.4% for supersonic flight. The center of gravity of the aircraft at takeoff conditions is at 116 feet (out of the 200 ft length). This leads to a static margin of 33.3% MAC. This case is presented in Figure 40. Considering that transport aircraft are usually designed with a static margin of 20% MAC or larger, the static margin at takeoff is acceptable.

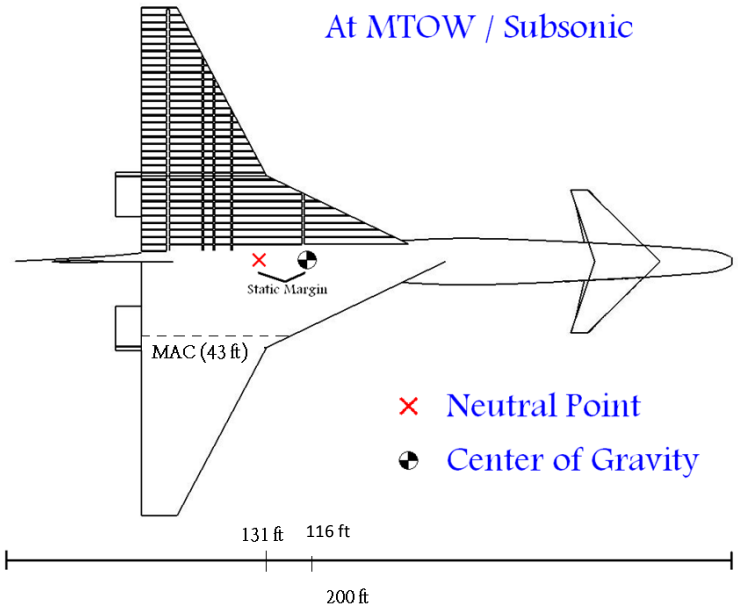

Figure 40: Static Margin Location

However, the center of gravity and neutral point will change based on fuel consumed and flight conditions. Therefore, the static margin will also change during flight, and it is important that that it stays within an acceptable envelope. The easiest way to maintain the static margin at a reasonable value is to drain the fuel tanks in a specific order, as discussed earlier. Considering

the high weight of the fuel, draining certain tanks can result in a substantial change in the center of gravity. For example, we are able to achieve a static margin of 31.2% MAC at the start of supersonic cruise, and a static margin of 28.0% at landing, both of which are acceptable for a transport aircraft.

Control Surface Sizing

Instead of using elevators and ailerons, we decided to employ elevons. Elevons are a type of control surface that combines pitch and roll. They are typically used on delta wing and tailless aircraft. Figure 41shows how elevons combine the functions of elevators and ailerons into one control surface[19].

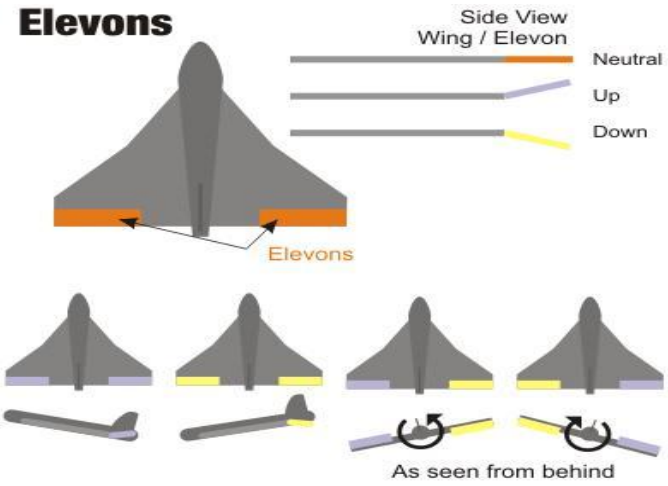

Figure 41: Elevons

Raymer[1] suggests that control surface sizing be done based on historical data. Using this method and including delta wing aircraft into his historical data, the elevons were sized at 310 ft^2 (total area for both sides). In comparison, the somewhat larger and heavier Concorde has a total elevon size of 345 ft^2 [4].

The sizing of the rudder (and therefore the tail) is slightly more complicated. The rudder size had to be able to meet the following three conditions: maintain lateral trim with one-engine out, landing in a 35 knot crosswind, and be comparable in size to rudders on other aircraft (with aircraft size taken into account). The first two conditions are essential because they both present a case where there is a significant yawing moment. The rudder has to be able to provide enough control to counteract these yawing moments. The third condition is there to ensure the feasibility of the rudder size. The rudder size that meets all of these conditions is 140 ft^2. For comparison, the size of the rudder on the Concorde is 112 ft^2[4].

Cost Analysis

RDT&E Cost

For the cost analysis, a modified RAND DAPCA IV cost estimation model is used. This model is shown in the "Aircraft Design: A Conceptual Approach" by Raymer[1] (pp 568-575). The cost model uses empty weight, maximum velocity, total length and other physical specifications to estimate the total research, development, testing and evaluation (RDT&E) cost. The following is a list of all the necessary inputs.

For the cost analysis, a modified RAND DAPCA IV cost estimation model is used. This model is shown in. The cost model uses empty weight, maximum velocity, total length and other physical specifications to estimate the total research, development, testing and evaluation (RDT&E) cost. The following is a list of all the necessary inputs.

Symbol	Name	Value
W_e	A/C Empty weight (lb)	117,740
V	Maximum velocity (knots)	1146
Q	Number to be produced in five years	30 (until 2020's, 100 A/C is to produced)
FTA	Number of flight-test aircraft	6
N_{eng}	Total production quantity times number of engines per aircraft	400
T_{max}	Engine maximum thrust (lb)	38500
M_{max}	Engine maximum Mach number	2
$T_{turbine\ inlet}$	Turbine inlet temperature (R)	3200
$C_{avionics}$	Avionics cost	$879,600,000

Table 11: Input parameters for cost calculation

The sizing code gave detailed values for the above inputs. The Q stands for lesser number of either total productions quantity or number aircrafts to be produced within five years. Since the total production quantity is 100 aircrafts, the quantity to be produced in five years is smaller. Assuming that the production slowly starts in the beginning, and later more aircrafts can be made faster, the number 30 is estimated as Q. The Supersonix aircraft is a complex product, thus, it will take more time in the beginning, and gradually manufacturers will be able to produce faster. The avionics cost was estimated using Raymer[1] (pp 568-575), which suggested using dollar between $3000 and $6000 per pounds of avionics. Thus, avionic cost is avionics weight, which is 1,444 pounds, multiplied by the upper limit, $6000 because the Supersonix will have sophisticated avionics system. For the engine cost, the maximum thrust is estimated from engine performance prediction method previously discussed. The turbine inlet temperature is

assumed to 3200 R. This value is assumed to be standard in current avionic technology level. The advancement of material technology allows turbine inlet to have higher temperature sustainability.

These input values are used with the hour equations from Raymer. These equations find required engineering, tooling, manufacturing, quality control hours, development support costs, flight test costs, manufacturing material costs, and engine production costs. The hour values are multiplied with their corresponding hourly rates. For the hourly costs, following values are used: (it is assumed that amount of hourly rate stays the same for 2009 year but inflation factor is factored in to preserve the value of 1999 dollars)

Work Type	Hourly Rate (1999 dollar)
Engineering	$ 86
Tooling	$ 88
Quality Control	$ 81
Manufacturing	$ 73

Table 12: Hourly rates

Multiplying the hourly rate with required hours and summing them up result in the RDT&E and flyaway cost. However, the DAPCA is based on design of an aluminum aircraft. A "fudge factor" of 1.3 is multiplied to the total cost to produce a more reasonable value. Supersonix aircraft will use substantial amount of graphite-epoxy based materials. There is also need to account cost for interior investment. Since Supersonix is a jet transport, $2500 per passenger per aircraft is added. The cost for interior is $15 million. The "investment cost factor" is multiplied to the total cost. This investment cost factor accounts for the cost of money and the contractor profit, so 1.2 is multiplied to the total cost.

The resulting total cost is based on 1999 dollars, so the inflation factor is multiplied to the cost. From the CPI database, $1 in 1999 has same value as $1.28 in 2009. To approximate the inflation to 2020, NASA's inflation prediction is used. The NASA calculator estimated $1.568 in 2020 having same value as $1 of 1999.

Finally, the RDT&E cost is $29 billion in 2009 dollars and $35 billion in 2020 dollars for producing 100 aircraft.

Direct Operating Costs (DOC)

The direct operating cost consists of fuel, crew, maintenance, materials, parts, and insurance costs. The DOC is calculated based on a one way trip from JFK to LHR.

First, the fuel cost is estimated based on the current cost of Jet A fuel. Currently, the fuel costs $57.03 per barrel. Based on the range from JFK to LHR, the distance is around 3000 nmi. The

estimate fuel cost for a one way trip is found to be around $17,000 in 2009 dollars. This value is based on a projected 2009 fuel price. Since fuel cost fluctuates greatly, this is a very rough estimate. It is likely that these costs will not exactly match year 2020 operation costs.

The estimation for crew cost is based on three-man-crew mode. The flight block hour is highly related to crew work hours. The crew cost contains wages for pilots and flight attendants. The average flight hour for trip is around five hours. Thus, the block time is five hours. Using the equation provided in the textbook, the estimated crew cost is $5,800 per flight in 2009 dollars**.**

Next, there are maintenance costs to ensure safety and regulatory compliance for every flight. The maintenance cost consists primarily of wages for technicians and engineers. The estimated man-maintenance-hour per flight hour is five. This estimate is found in Raymer[1](Table 18.1, p571). The maintenance cost is found by multiplying maintenance-man-hour per flight hour with estimated hour wage. The estimated maintenance cost per year per aircraft is $3,300,000 in 2009 dollars. This is comparable to the maintenance cost of F-18, which is also supersonic. The cost is about $3 million dollars per year per aircraft.

There are also parts and material costs associated with maintenance. These costs cover the cost necessary replacement parts, and they relate to the cost of the aircraft. The material costs depend on the flight hour and the cycle. Every cycle or trip, the aircraft goes through routine inspections, and if repair is needed, the parts and components will be purchased. The material costs are estimated using the equation indicated in Raymer[1](Table 18.1, p573). The material cost is estimated to be $17 million (2009 dollars) per year. This cost is very high since Supersonix will use advanced materials and advanced avionics.

Insurance costs can be estimated by multiplying the total DOC by 10%. Surmising all the costs, the total DOC for the JFK to LHR trip is $ 0.20 per set-mi. This is in 2009 dollars. This can be compared to the typical DOC of jet aircraft. Raymer has indicated in his book that the average cost is about $0.04. This makes the DOC of Supersonix 500% more expensive than the average. However, the average value of four cents is based on subsonic aircraft. Also the economic conditions and the fuel prices could be significantly different from year 1999.Thus accounting steep rise of fuel cost, the DOC is relatively an acceptable value, which is $0.20 per seat-mile.

Indirect Operating Costs (IOC)

Indirect operating costs are expenditures occurring during service that are not covered in the DOC. Some IOC examples are landing fees, management fees, and also the cost of the money. Landing fees are paid to the airport for using the runways. This cost is based on the maximum takeoff weight of the aircraft; however, the landing fee varies for different airports. For example, the landing fee for Super Sonix at JFK airport is $1700, but only $860 at LHR. The IOC is difficult to determine accurately due to IOC is mostly independent from aircraft design. The

textbook states that IOC ranges from one third of the DOC to whole DOC. Therefore, the estimated IOC is equal to the DOC, meaning $0.20 per seat-mi for a one way trip from New York to London.

Cost Summary

It is stressed that this is rough estimation of the costs. Also note that the cost model is decade old. About one hundred aircraft will be manufactured, yielding an individual price of $290 million per airplane. This is comparable to the price of Concorde before retirement after factoring in the inflation. The cost of Concorde would be around $250 million if it was available for purchase today (2009) if the value of Concorde stayed same. Finally, a table of all the cost values is shown below.

Costs	Value (2009 dollars)
RDT&E Cost	$29 billion
Direct Operating Cost	$0.20 per seat-mile
Indirect Operating Cost	$0.07 – 0.20 per seat-mile
Procurement cost of a Concorde	$250 million
Procurement cost of a Supersonix	$290 million

Table 13: Cost Summary

Summary

A complete conceptual design has been performed for a small supersonic airliner with Initial Operating Capability in 2020. At the very beginning, the feasibility of this endeavor from a consumer viewpoint was considered in the Systems Requirements Review: potential market and customers were analyzed to determine the demand for this transport; their requirements and desired engineering characteristics were assimilated into the House of Quality to help guide the design process; a typical concept of operations was drawn up to determine the design mission for the aircraft. The aircraft took on a more technical definition in the Systems Definition review: performance constraints were imposed to get a general idea of aircraft parameters; Concepts were generated using Pugh's method to sort organize the ideas methodically. Finally, to complete the conceptual design, the Conceptual Design Review is performed: A detailed sizing code is developed that allows the optimization of the aircraft; various aspects of the properly sized aircraft such as weights and balance, structures and costs are analyzed to crystallize the aircraft concept further. Now, after having gone into a great detail to define the Supersonix aircraft concept, the plausibility for further development work must be evaluated.

The answer to this question begins with the Requirements Compliance Matrix. This matrix contains much of the design goals that the Supersonix aircraft has to meet, and tracks the

evolution of the aircraft concept right from the early stages of simple sizing. The latest version of this matrix is displayed in Table 14. All of the aircraft performance targets, such as cruise Mach number, takeoff and landing field lengths, number of passengers and design range have been met and exceeded. One of the most important requirements is the sonic boom overpressure, and the achievement of this target allows the Supersonix aircraft to fly its design mission effectively according to the concept of operations. As a tradeoff, the cruise altitude had to be increased to 60,000ft in order to accommodate the low overpressure. The elevation of the cruise altitude means a heavier fuselage structure to withstand the larger pressure differential, but also means less drag and a more efficient fuel burn. Therefore the fact that this requirement was not met does not have a large negative effect to the Supersonix aircraft.

Compliance Matrix

Requirements	Target	Threshold	Direction of Improvement	Value	Requirement Units
Take off length	8400	10000	↓	2877	ft
Landing field length	8400	10000	↓	1866	ft
Door height above ground	8	10		10	ft
Turnaround time	0.5	1	↓	1	hr
range	5000	4000	↑	4500	nm
# passenger	60	50	↑	60	people
Cruise Mach number	2	1.6		1.8	Mach
cabin valume per pax	65	50	↑	65	ft^3/pax
Operating cost	--	--	↓	0.2	dollars/ASM
Cruise Altitude	50000	40000		60000	ft
Cruise Efficiency	3	3	↑	2.89	pax-mi/lb fuel
Sonic boom overpressure	0.3	0.3	↓	0.28	lb/ft^2
Cumulative Certification noise	60	80	↓	--	dB
Second Segment climb gradient	2.6	2.4	↑	3	%

Table 14: Requirements Compliance Matrix

One target that was not met was the cruise efficiency of 3 pax-mi/lb fuel. The Supersonix aircraft is able to come close to that value, with the cruise efficiency being 2.89 pax-mi/lb fuel. The slight decrease in the efficiency can be attributed to the additional wave drag generated by the blunt nose in order to minimize the sonic boom overpressure. It is expected that further research and development of this concept can and will bring the fuel efficiency up and perhaps even exceed the target.

Finally, the cumulative certification noise was to be below 80 dB; at this stage of conceptual design, there is no reliable, consistent way of predicting the noise emitted from the aircraft. Therefore, although the design of the aircraft included the consideration of minimizing the

noise footprint of the aircraft, it is not possible to tell if the aircraft meets this target at this point.

Therefore, the concept of a small supersonic transport is definitely worth pursuing to the preliminary design stage. There is a market for supersonic transport, and potential customers and concept of operations have been identified. The engineering analysis suggests that, although not all of the requirements are met, the aircraft is very close to satisfying and perhaps even exceeding those goals. Technologically, it is expected that all of the skills and expertise required to implement the features on the Supersonix aircraft be ready by the time the aircraft is produced for IOC in 2020. The economy is anticipated to recover from the present-day situation and be ready to accept this revolutionary mode of travel.

Additional work

In-depth aerodynamic analysis must be further examined. Aerodynamic flow over the body is currently approximated and no shock interactions have been considered. Sonic boom signature must be examined more closely by applying area ruling at different mach angles from the front of the aircraft. Fuselage structures must be further researched to include specialized structural load path at location of high stress concentration. CATIA model of fuel tanks, cargo space, center of gravity travel (aircraft load configuration) must be finalized. Material selection should be inputted into CATIA providing a finalized moments about the x, y and z axis. The results from finalized CATIA model can be used to validate the dynamic stability and control of the aircraft. The results can provide a more accurate aircraft trim diagram as well mission performance. The aircraft response can then be plotted to provide transient response, delay time, and overshoot. These results will provide insight on further feasibility of the Super Sonix and more detailed cost analysis.

References

[1]. Raymer, D.P., *Aircraft Design: A Conceptual Approach*, AIAA Education Series, Fourth Edition

[2]. Harry W. Carlson, "Simplified Sonic-Boom Prediction," NASA Technical Paper 1122, 1978

[3]. Seebass, R. and George, A.R.,"Sonic-boom minimization" Cornell University, January 1971

[4]. Gordon, "Concorde, Celebrating an Aviation Icon", October, 2006 [http://www.concordesst.com. Accessed April, 2009]

[5]. Jumper, E. J., "Wave Drag Prediction Using a Simplified Supersonic Area Rule", Journal of Aircraft, Vol. 20, No. 10, October 1983, pp. 893-895

[6]. Lednicer, David, "The Incomplete Guide to Airfoil Usage,"Analytical Methods, Inc., *4/10/2007,* [http://www.ae.uiuc.edu/m-selig/ads/aircraft.html, Accessed March, 2009]

[7]. Feuillard, Philippe, "Chevron-type primary exhaust nozzle for aircraft turbofan engine," December 30, 2008 [http://www.patentgenius.com/patent/7469529.html, Accessed March, 2009]

[8]. Soltani, M. R., Farahani, M., and Younsi, J. S., "Performance Improvement of a Supersonic External Compression Inlet by Heat Source Addition," The proceedings of world academy of science, engineering and technology, Volume 30, July 2008

[9]. H & S, "Aviation Structural Mechanic, Aircraft Construction and Materials," [http://www.tpub.com/air/1.htm, Accessed 4/26/09]

[10]. "Concorde", [http://www.pilotfriend.com/photo_albums/potty/14.htm, Accessed 4/26/09]

[11]. National Materials Advisory Board (NMAB), *New Materials for Next Generation Commercial Transport*,pp.28, Washington D.C., National Academy Press, 1996

[12]. Professor C.T. Sun, 4/17/09

[13]. *Boeing Unveils 7E7 Fuselage Section*, Reinforced Plastic, Volume 49, Issue 2, Elsevier Ltd. 2005

[14]. Baker, Alan,et.al. *Composite Materials of Aircraft Structure*, 2nd Edition, Virginia, AIAA Education Series, 2004, pp 291

[15]. CES Selector, Granta Design Limited, United Kingdom, 2008

[16]. Sensmeier, M.D,Samareh,A.J., *A Study of Vehicle Structural Layouts in Post-WWII Aircraft*,45th AIAA/ASME/ASCE/AHS/ASC Structures. Structural Dynamics & Materials Conference, California, 2004

[17]. Cytec Engineered Materials, “FM 1000 Adhesive Film,” [http://www.cytec.com/engineered-materials/products/Datasheets/FM1000.pdf, Accessed 4/26/09]

[18]. Griffith, B., “Boeing sets pace for composite usage in large civil aircraft,” [http://www.compositesworld.com/articles/boeing-sets-pace-for-composite-usage-in-large-civil-aircraft.aspx, Accessed 4/26/09]

[19]. Michael James , “Elevons Are For Mixed Control” [*http://rcvehicles.about.com/od/rcairplanes/ss/RCAirplaneBasic_7.htm*, Accessed April, 2009]

[20]. Dippold, Vance III, “CFD Analyses and Jet-Noise Predictions of Chevron Nozzles With Vortex Stabilization” Glenn Research Center, Cleveland, Ohio

[21]. Roskam, J., *Airplane Flight Dynamics and Automated Flight Controls: Part I*, DAR Corporation, Lawrence, KS, 2001

Appendix

Engine Performance Curves (from Raymer App.E)

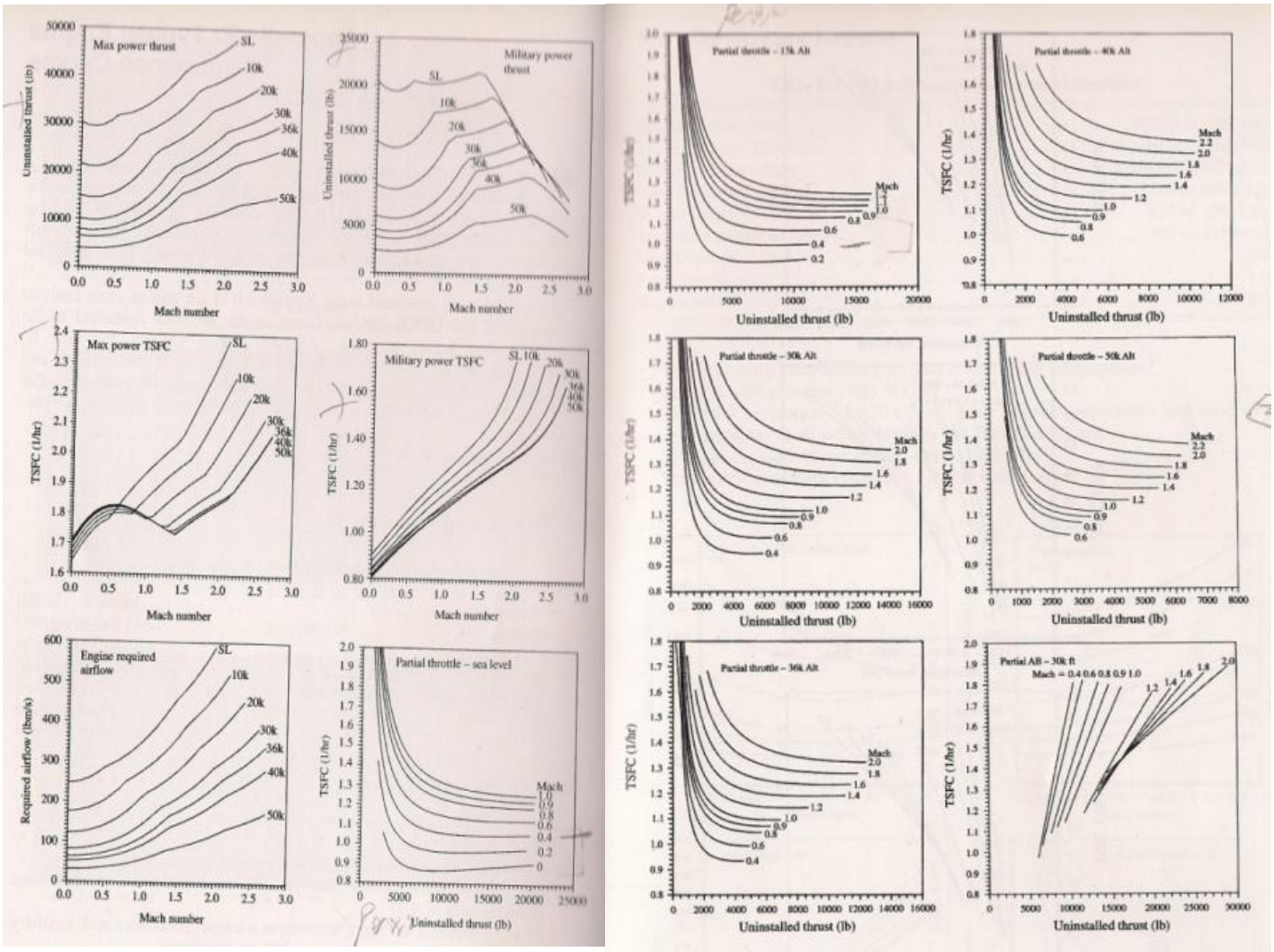

Composite carpet plot